Constraining the duration of ram pressure stripping from the direction of optical jellyfish galaxy tails

Vicente Horacio Salinas Froemel

Instituto de Física y Astronomía
Facultad de Ciencias

Universidad de Valparaíso
Doctorado en Astrofísica

Abril 2023
Valparaíso. Chile.

This thesis is solely my own composition,

except where specifically indicated in the text.

Vicente Horacio Salinas Froemel
April 2023.
Valparaíso. Chile.

Acknowledgements

I'm extremely grateful to Dr. Yara Jaffé, from who I learned the most thanks to her exceptional guidance throughout my time at UV thus far. I deeply appreciate Dr. Rory Smith and Dr. Jong-Ho Shinn for their enthusiasm to collaborate with us on this project. I would also like to thank the people from the jellyfish group at UV and everyone that took the time to participate in the classification of the galaxy tails. Special thanks to Dr. Jacob Crossett for sharing the initial tail classification script and Ana Lourenco for providing us with a lot of the data necessary to complete this work. I am also grateful to the GASP team, Dr. Marco Gullieuszik and Gemma González for sharing the Hα tail classifications.

Abstract

Within the field of galaxy evolution, we know the life of a galaxy can be driven by a combination of internal and external mechanisms. Amongst the latter, perhaps the most efficient mechanism affecting the gas content and star formation histories of galaxies in dense environments is ram pressure stripping, produced when a galaxy moves through the intergalactic medium within groups and clusters of galaxies. Extreme examples of on-going ram pressure stripping are known as jellyfish galaxies, a type of galaxy characterized by a tail of stripped material that can be directly observed in multiple wavelengths. Using the largest broad-band optical jellyfish candidate sample in local clusters known to date, we measure the angle between the direction of the tails visible in the galaxies, and the direction towards the host cluster center. We find that 32.7% of the galaxy tails point away from the cluster center, 18.5% point toward the cluster center, and 48.8% point elsewhere. Moreover, we find strong signatures of ram pressure stripping happening on galaxies pointing away and towards the cluster center, and larger velocity dispersion profiles for galaxies with tails pointing away. These results are consistent with a scenario where ram pressure stripping has a stronger effect for galaxies following radial orbits on first infall. The results also suggest that in many cases, radially infalling galaxies are able to retain their tails after pericenter and continue to experience significant on-going ram pressure stripping. With the observational measures obtained in this work, we then constrain the lifetime of the optical tails from the moment they first appear to the moment they disappear, by comparing them with N-body simulations in combination with an MCMC model. We obtain that galaxy tails appear for the first time at ~ 1.16 R_{200} and disappear ~ 650 Myr after pericenter. Finally, this work constitutes an important base for future studies with increasingly larger samples of ram pressure stripped galaxies.

Contents

1 Introduction **1**

1.1 Cosmology and galaxy formation 1

1.2 Galaxy evolution 2

1.3 The effect of the environment in galaxy evolution 3

1.3.1 The group and cluster environment 3

1.3.2 Environmental mechanisms 5

1.3.3 Ram pressure stripping 7

1.3.4 Jellyfish galaxies 9

1.3.5 Phase-space diagrams as a tool to understand ram pressure stripping 11

1.3.6 Tail directions of jellyfish galaxies 13

1.4 This thesis 14

2 Data and Method **17**

2.1 Sample and data 17

2.2 Measuring the tail directions of jellyfish galaxies 19

3 Results **25**

3.1 Comparison with Hα 25

3.2 Tail angle distribution 28

3.2.1 Overall tail angle distribution 28

3.2.2 Tail angle distribution for different coverages 32

3.3 Phase-space distribution 35

3.4 Radial distribution 38

3.5 Dependence of tail angle on cluster and galaxy properties 40

3.5.1 Dependance on cluster and galaxy mass 40

3.5.2 Dependance on color 41

3.6 Lifetime of optical tails in stripped galaxies 44

4 Summary and Conclusions **49**

5 Future Perspectives **53**

A Appendix: Tail Measurements **55**

Chapter 1

Introduction

1.1 Cosmology and galaxy formation

The key factors to understanding galaxy formation are the initial conditions of the Universe, and how these initial conditions evolve over time. Knowing both would give us the recipe that creates the Universe as we observe it today. While many questions are still in need of an answer, one thing we know is that galaxies would not have been formed if the Universe was completely uniform and isotropic. This, as well as other pieces of evidence such as the anisotropies in the cosmic microwave background (Mather et al. 1990, Planck Collaboration et al. 2020), tells us about the existence of primordial density fluctuations. These are small density variations in the early Universe that we believe were caused by quantum fluctuations during inflation (Guth 1981, Sasaki 1986), a period of exponential expansion of the Universe. After inflation the Universe continued its expansion gradually, amplifying the initial density fluctuations and becoming cooler. At a point matter became cool enough for gravity to begin the process of gravitational collapse in the overdense regions, allowing the formation of structure (Peebles & Yu, 1970).

Within the context of the Lambda Cold Dark Matter (ΛCDM) model (Peebles, 1984), dark matter decouples from the radiation field before baryonic matter and begins to collapse onto dark matter halos. As the Universe cooled further the baryons followed dark matter, collapsing into the dark matter halos, where the gas became

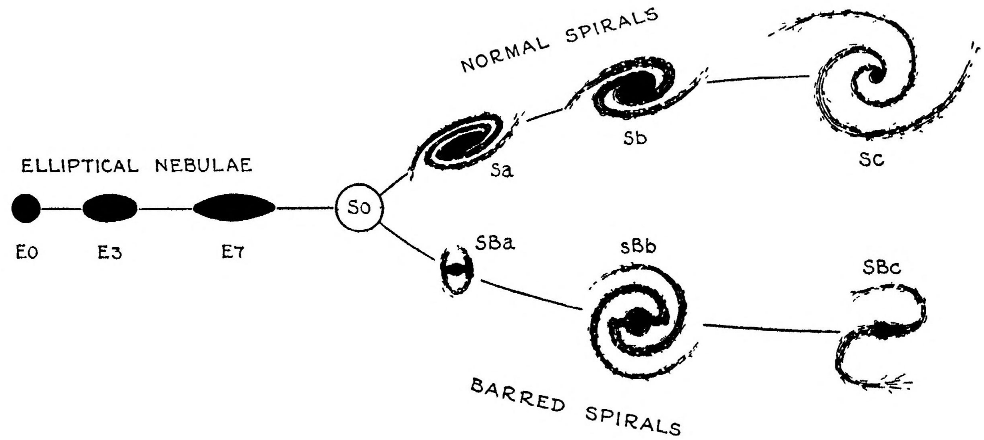

Figure 1.1: Original Hubble sequence from Hubble (1936). From left to right in the diagram, the galaxies go from early-type to late-type galaxies.

dense and cool enough to begin star formation, giving birth to the first generation of galaxies. Dark matter halos would then continue to grow as smaller halos merge with each other in a bottom-up scenario (White & Rees, 1978), causing galaxies to merge and form bigger galaxies, and to group together into galaxy groups and galaxy clusters.

1.2 Galaxy evolution

A galaxy is defined as a collection of stars, gas, dust, and dark matter that is bound by gravity, but the distribution and properties of the contents in these collections can widely vary. This poses a challenge for evolutionary models, as they need to be able to explain the differences and reproduce the observed fractions of the different galaxy types. A major step to accomplish this was to identify and categorize galaxies by morphology. The most popular scheme is the one proposed by Hubble (1926,1936) seen in Figure 1.1. He arranged galaxies in a sequence going from more spheroidal galaxies to more disk-like galaxies, with a scheme that has two main galaxy types; elliptical and spiral galaxies. The former have spheroidal shapes and the latter consists of a disk with characteristic spiral arms. Spirals can have a bar-shaped structure at the center, in which case they enter a second subcategory, called barred spiral galaxies. There are also lenticular galaxies, which are an intermediate type between spirals and ellipticals, and irregular galaxies, which do not have a distinctive shape. Hubble introduced the concept of "early" and "late" types, starting in the sequence from more roundish elliptical galaxies, and then to spirals with more opened arms and irregulars. In general, the set of elliptical and lenticulars is referred to as early-type galaxies, and the set of spirals and irregulars is called late-type galaxies.

The Hubble sequence went through further refinements and additions to include other and more specific types of galaxies, but the general early-type versus late-type scheme remains heavily used today. Numerous studies have established that early-type galaxies are characterized by having low gas content and low star formation rates, which gives them their red colors, characteristic of old stellar populations, while late-type galaxies typically have high star formation rates, blue colors, and young stellar populations. This correlates with the gas content of a galaxy, which fuels star formation and allows for new stars to be born. In another respect, ellipticals are dominated by the velocity dispersion of their stars, in contrast with spirals, which instead need a high angular momentum to maintain their disk-like structure. Ellipticals are also more massive on average, suggesting a larger count of merger events, which can be responsible for the large velocity dispersions as well. Many times mergers are invoked as responsible for the apparent transformation of spiral galaxies into elliptical galaxies since it has been shown through simulations that mergers of two galaxies can potentially result in a galaxy with very different properties from their progenitors (e.g. Toomre & Toomre, 1972, Walker et al. 1996). However, while these systematic differences give us clues about the evolutionary paths of galaxies, one should be aware that these trends describe a general picture, with many exceptions observed (e.g. blue ellipticals, passive spirals, massive spirals) that also need to be accounted for when modeling galaxy evolution.

1.3 The effect of the environment in galaxy evolution

1.3.1 The group and cluster environment

Galaxy clusters and galaxy groups are collections of galaxies bounded by gravity. Groups can have less than ~ 50 members, while clusters can be much larger, ranging from hundreds to thousands of members. These collections are believed to be embedded in extended dark matter halos, which can be sometimes traced using gravitational

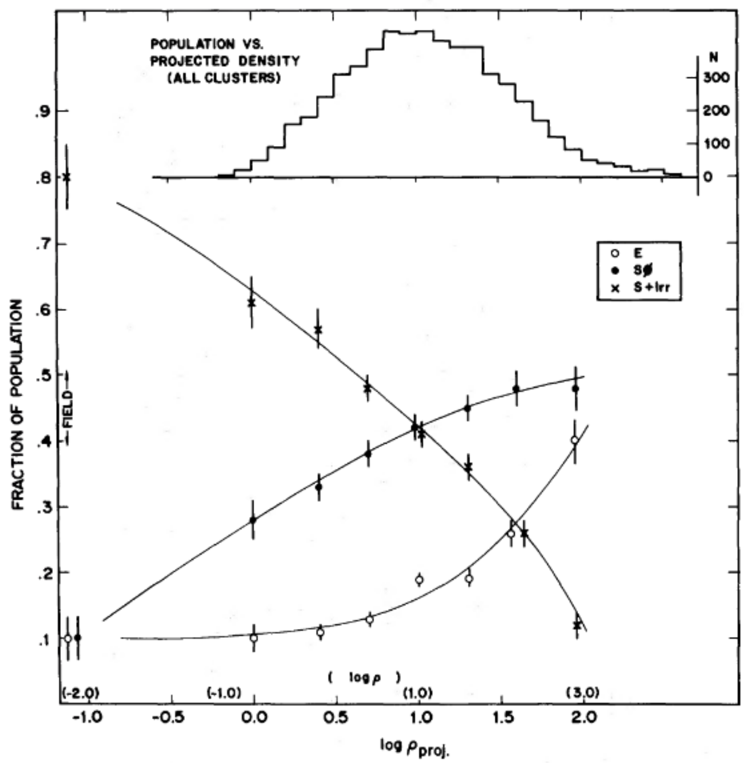

Figure 1.2: Fractions of galaxy populations vs. density of projected galaxies (Dressler, 1980). Open circles are elliptical galaxies (E), filled circles are lenticular galaxies (S0), and crosses are spirals plus irregular galaxies (S+Irr).

lensing techniques. The space between the galaxies is also filled with hot gas, known as the intracluster medium (ICM), or intragroup medium in the case of groups. This hot gas produces x-ray emission that allows us to trace it directly (unlike the case with dark matter), which is one way to identify clusters in the first place. Typically, around $\sim 80 - 90\%$ of the matter content in clusters is dark matter, $\sim 10 - 15\%$ is from the ICM, and only less than $\sim 1\%$ belongs to galaxies (Lin & Mohr 2004, Gonzalez et al. 2007). Near the bottom of the potential well of a cluster, we can typically find the brightest cluster galaxy (BCG), which is usually a massive elliptical galaxy (including the most massive examples in the Universe).

The galaxy populations in clusters are different from the field (i.e. galaxies that do not belong to a group or cluster), as evidenced by Dressler (1980), who studied galaxy populations as a function of galaxy density (see Figure 1.2), finding that the population of early-type galaxies increases in more dense environments, while the fraction of the spiral population decreases. This is known as the morphology-density relation and serves as the primary piece of evidence that galaxies evolve differently depending on the environment. Later works obtain consistent evidence with this scenario, such as in Whitmore et al. (1993), where they find the fraction of early-type galaxies increases with lower clustercentric radius, and Gavazzi et al. (2010) where they find redder colors in denser environments. Properties associated with early-type galaxies, such as low gas content, are also observed in late-type galaxies in clusters. In Davies & Lewis (1973) they study galaxies in the Virgo cluster, finding a deficit of neutral atomic hydrogen (HI) across all morphological types. At the time they attributed this result to a higher likelihood of galaxy mergers in clusters than in the field, which could potentially remove the gas in galaxies. However, today we know galaxy velocities in clusters are too high for galaxy mergers to exclusively explain this result since merger rates are disfavoured in environments with high-velocity dispersion (Ostriker 1980, Makino & Hut 1997). Alternatively, hydrodynamical effects were just beginning to be considered as possible mechanisms for gas stripping in dense mediums (Gunn & Gott, 1972). A quantitative definition of the HI deficit was created in Giovanelli & Haynes (1985), where they once again find that galaxies in clusters lack HI when compared with galaxies of similar Hubble types in the field. It is then natural to expect lower star formation rates from galaxies in clusters, and this is corroborated by the work of Kennicutt (1983), in which they use the Hα emission to compute the star formation rates of galaxies from the Virgo cluster, finding low star formation rates, as well as low HI contents. Recent works are also consistent with this picture (Solanes et al. 2001, Boselli & Gavazzi 2006, Haines et al. 2015, Jaffé et al. 2016).

All these findings lead us to the conclusion that galaxies in dense environments must experience certain conditions that tend to evolve them into early-type galaxies more rapidly than in the field, and that the gas content is the main component being affected. The question that follows is what are the different physical mechanisms quenching galaxies in different environments, their relative role, and their effects on galaxies?

1.3.2 Environmental mechanisms

The observations clearly indicate that galaxies in dense environments are experiencing enhanced halting of the star formation, also known as quenching (see Boselli & Gavazzi 2006 and Cortese et al. 2021 for a complete review). Therefore, when studying possible mechanisms, one of the main objectives is to understand their effect on the gas content of galaxies. In Figure 1.3 we present an illustration from Cortese et al. (2021), in which we can appreciate different quenching paths and effects on the cold gas in the interstellar medium (ISM) of a galaxy. Simply put, a galaxy will have effective star formation if dense and cold gas is available. Therefore, the simplest and most natural way for a galaxy to become quenched is by consuming all the available gas, or by halting the accretion of new gas from the circumgalactic medium. This phenomenon is known as starvation (Larson et al., 1980) and is typically a necessary condition for galaxies to remain passive. Another alternative is that instead of an absence of gas, the existing gas is unable to effectively start the process of star formation because of low densities and/or hot temperatures. An example of the former are low surface brightness galaxies, where the densities in the ISM are lower than in normal galaxies, making gravitational collapse less likely to occur. Heating of the ISM can occur via outflows of gas, caused by internal mechanisms such as AGN feedback, supernovae feedback, or stellar winds. These processes could also remove some of the gas as well, further enhancing the quenching process. Indeed, the fastest way for a galaxy to become quenched is by directly removing the gas from the disk. However, while internal mechanisms can play a role in this process, they are not enough to explain the gas deficiencies observed in clusters and groups, since satellite galaxies typically have lower gas content than central galaxies in groups at fixed stellar mass (van den Bosch et al. 2008, Davies et al. 2019).

In general, the mechanisms driving the evolution of a galaxy can be divided into two types of factors. On the one hand, we have the internal factors coming from within a galaxy that occur naturally as a result of the galaxy's own processes (gravitational instabilities, AGN feedback, supernovae feedback). The evolution of galaxies from the field or central galaxies in groups is thought to be mainly driven by some of these non-environmental mechanisms. On the other hand, we have the external factors caused by the interactions between a galaxy and its environment. These kinds of mechanisms can be further divided into two categories; gravitational effects (e.g. galaxy-galaxy interactions, galaxy-cluster interactions, harassment), and hydrodynamical effects (e.g. ram pressure, thermal evaporation, viscous stripping) caused by the interactions with the medium surrounding a galaxy. The main difference between gravitational and hydrodynamical effects is that the former is capable of perturbing the stellar content, while the latter can only directly perturb the gas content. However, both effects are capable of stripping large quantities of gas from galaxies, making them the primary suspects to explain the enhanced quenching in dense environments. Furthermore,

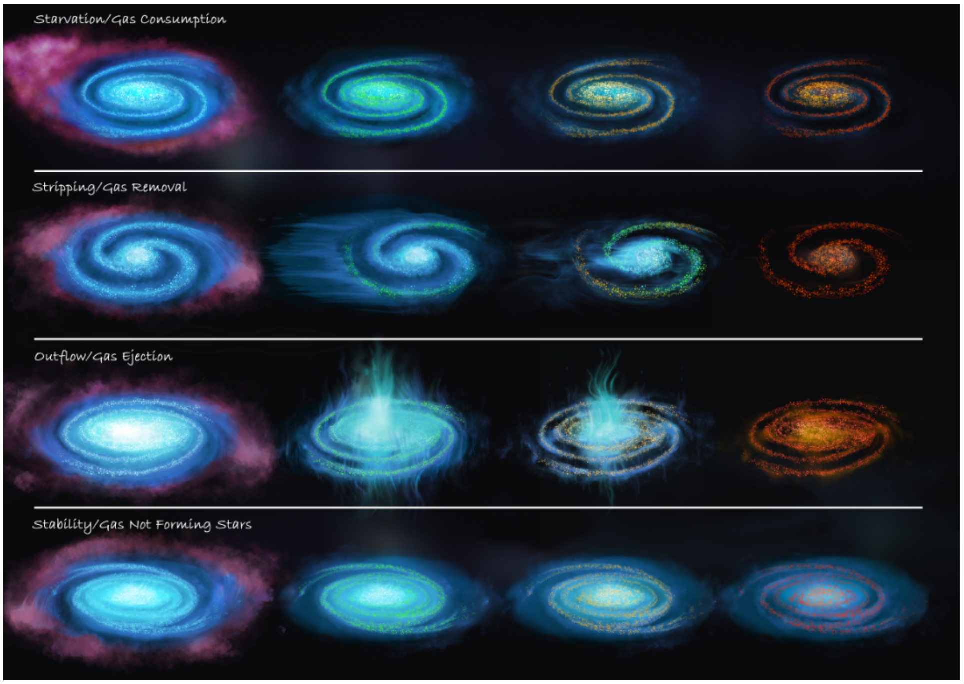

Figure 1.3: Illustration of possible quenching pathways from Cortese et al. (2021). The circumgalactic medium surrounding a galaxy is represented in pink, the ISM is represented in blue, and stars are represented as dots with colors ranging from blue to red to indicate younger and older populations, respectively.

these factors could be happening simultaneously on a galaxy, and even boost some of the others. For example, external effects could alter the efficiency of internal mechanisms, by feeding extra material into an AGN (Poggianti et al. 2017a, Reeves et al. 2022) or by triggering gravitational instabilities (Schulz & Struck, 2001). Sometimes the presence of many factors affecting a galaxy can complicate the study of individual mechanisms since different mechanisms could have similar observable effects on a galaxy.

1.3.3 Ram pressure stripping

Ram pressure stripping is the most studied hydrodynamical effect, and possibly the one with the greatest impact on the gas content of cluster galaxies. This process occurs when a galaxy moves through a dense medium, such as the ICM in clusters. As the galaxy moves through the medium, it experiences a drag force capable of stripping some (or all) of the gas in the ISM. A simple formalism that attempts to quantify this force was proposed by Gunn & Gott (1972), where the ram pressure is given by

$$P_{\rm ram} \approx \rho_{\rm e} v^2, \tag{1.1}$$

where $\rho_{\rm e}$ is the density of the medium, and v is the velocity of the galaxy relative to the medium. In other words, galaxies moving fast through a dense medium will experience higher ram pressure than galaxies moving slowly or in a low-density medium. This mechanism can effectively affect the gas component if the force produced by ram pressure surpasses the binding force of the galaxy. However, the existing stellar component is expected to remain mostly unaltered by this process (albeit not completely, see Smith et al. 2012), since it has a strong bound to the gravitational potential well of the galaxy. We should also note that this formalism is a simplification, since there are other factors, such as the inclination of the galaxy relative to the direction of motion, that influence how much gas can be effectively removed. Other hydrodynamical mechanisms, such as thermal evaporation (Cowie & Songaila, 1977) and viscous stripping (Nulsen, 1982), might also be at play to aid the gas removal.

Outside the theoretical standpoint, it took some time for observational evidence of ram pressure stripping to become evident, since mergers were also capable of reproducing the observed gas deficiencies. The works of Dressler (1986) and Giraud (1986) provided some of the first indirect evidence of ram pressure stripping being a key mechanism acting in clusters. By studying the orbits and HI deficiencies of cluster galaxies, they find that galaxies in more radial orbits, which would be capable of reaching higher velocities and lower clustercentric distances (i.e. higher ram pressure according to Equation 1.1), seemed to be more gas deficient than galaxies in more circular orbits. However, the smoking gun would appear when radio interferometers allowed for high-resolution observations of HI distributions. HI maps from Warmels (1988) and Cayatte et al. (1990) show that cluster galaxies have less extended distributions than isolated galaxies of similar morphologies. This result is consistent with an outside-in truncation of the gaseous disk, with the stellar component remaining unaffected. This is exactly what one would expect from ram pressure stripping. Furthermore, direct evidence of on-going stripping became available with the discovery of the so-called jellyfish galaxies (e.g. Gavazzi et al. 1995, Chung et al. 2009).

1.3.4 Jellyfish galaxies

When gas in the ISM is being removed from a galaxy by ram pressure it can leave behind a trail of material opposite to the direction of motion of the galaxy, which can be directly traced in a multitude of wavelengths, such as radio emission. This results in a galaxy with a tentacle-like structure, known as the tail. This peculiar morphology is what inspired the term of jellyfish to refer to these galaxies. Nowadays, a galaxy showing any sign of on-going ram pressure stripping can be considered a jellyfish candidate. One way to identify a jellyfish galaxy is by confirming the presence of a radio tail. However, remarkable properties have been observed in other wavelengths as well; when inspecting the Hα emission (which traces star-forming regions), jellyfish galaxies show an asymmetric distribution that appears to follow the general direction of the radio tails (Gavazzi et al., 1995), often showing knots of star-forming regions within the tail (see Figure 1.4). Jellyfish galaxies sometimes show a bow-shock (or "u-bend") structure in the side opposite to the tail direction, further resembling the head of a jellyfish. UV and short optical wavelength observations (tracing the young stellar population) have also been shown to have similar morphologies. However, the old stellar population of these galaxies appears unaltered, as evidenced by their near-IR emission in Gavazzi et al. (1995).

Quenching of the star formation is expected from the removal of the gas in galaxies that have already been stripped. However, the asymmetry of the young stellar population, plus higher specific star formation rates in the main body of some jellyfish galaxies compared to normal galaxies (Gavazzi et al., 1995), lead us to believe that galaxies undergoing ram pressure stripping experience a short-term enhancement of the star formation activity caused by the compression of gas due to ram pressure. This is further supported by N-body hydrodynamical simulations from Kronberger et al. (2008) (although the predictions were too extreme compared to the observations), and by the latest statistical studies on jellyfish galaxies (e.g. Poggianti et al. 2016, Vulcani et al. 2018, Lee et al. 2022).

Although individual examples of jellyfish galaxies have been observed for a relatively long time, large samples of jellyfish galaxies have only recently started to appear, starting with the works of McPartland et al. (2016) and Poggianti et al. (2016) (hereafter P16). With these works, we began to more confidently define some of the common properties of these galaxies, and in turn, better understand the effects of ram pressure stripping. As we will see in the following sections and throughout this work,

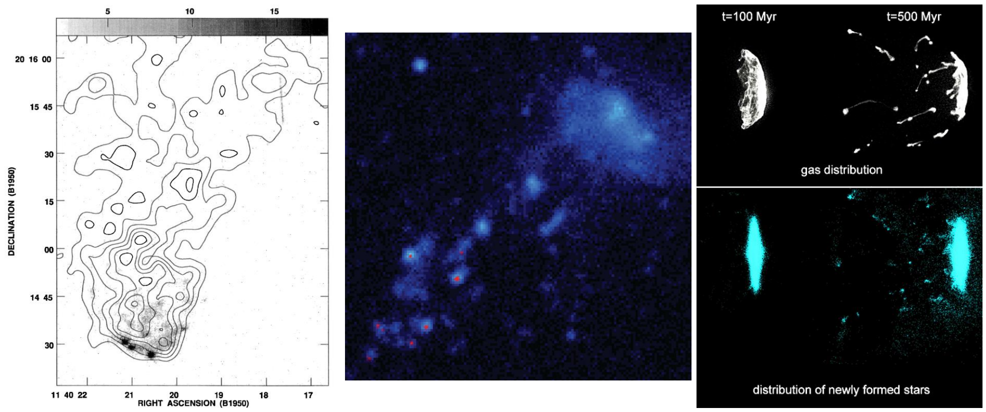

Figure 1.4: Examples of jellyfish galaxies from the literature. Left: Radio continuum contours superposed to gray scale Hα emission of the jellyfish galaxy GCG 97-073, from Gavazzi et al. 1995. Middle: Hα+[N$_{II}$] (red) plus near-UV (blue) image of the jellyfish galaxy IC3418, from Kenney et al. 2014. Right: Distribution of the gas (white) and newly formed stars (turquoise) seen edge-on for a simulated ram pressure affected galaxy, which moves face-on through the ICM, after 100 Myr (left side) and after 500 Myr (right side), taken from Kronberger et al. (2008).

we can use these galaxies to help constrain the parameters that govern galaxy evolution in dense environments.

From the P16 sample, the GASP project (Poggianti et al., 2017b) also emerged, using the MUSE instrument to target the jellyfish galaxies. As a result of this survey, another potential property of jellyfish galaxies was discovered, which is the apparent unwinding of the spiral arms. This was first observed in the jellyfish galaxy JO201 (Bellhouse et al., 2017), and shortly after observed in ten more jellyfish candidates from the P16 sample (Bellhouse et al., 2021). However, this unwinding feature is observed in only a few confirmed jellyfish galaxies and could be caused by other mechanisms, such as gravitational effects. Whether or not this feature can be exclusively caused by ram pressure stripping remains a subject of debate today. The recent work of Vulcani et al. (2022) identifies a large complementary sample of unwinding galaxies (see Figure 1.5) from the same clusters in P16, but at the moment they can not establish how often the observed features are due to ram pressure stripping. They also provide the latest fraction of optical jellyfish galaxies, being $\sim$ 15% of the blue, non-interacting cluster population if we do not include the unwinding sample and up to $\sim$ 35% if we consider all unwinding galaxies as jellyfish galaxies.

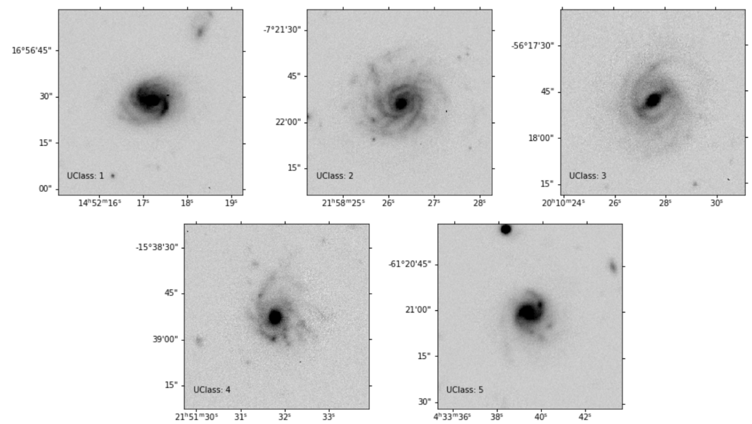

Figure 1.5: Optical examples of unwinding galaxies from Vulcani et al. (2022). They are classified by "Unwinding Class" (UClass) denoting visual evidence for unwinding of the spiral arms, from extreme cases (UClass 5) to progressively weaker cases, down to UClass 1.

1.3.5 Phase-space diagrams as a tool to understand ram pressure stripping

To study ram pressure and the continuously growing samples of jellyfish galaxies, some commonly used tools have been developed. One that is extremely useful to understand ram pressure stripping are velocity versus position phase-space diagrams since they contain information relating to both components of Equation 1.1.

In Figure 1.6 we show some examples of these diagrams from Jaffé et al. (2018). In the left panel, we show the result of a simulation to highlight the different regions of the diagram. When a galaxy is entering a cluster for the first time it will typically locate at the "recent infalls" region, characterized by medium to large velocities and cluster-centric distances. As a galaxy falls into the cluster it will gain speed and get closer to the cluster center, entering regions where ram pressure stripping begins to become effective (upper left regions in the diagram). The galaxies that would experience the strongest stripping should be the ones capable of reaching the highest velocities and getting the nearest to the cluster center, where the density is the highest. Therefore, we expect these galaxies to be in mostly radial orbits that fall directly into the cluster as opposed to more stable circular orbits. After the first pericenter passage, galaxies would then move away from the cluster center and start to slow down. This cycle would repeat, further lowering the velocity until the galaxy reaches a stable orbit and becomes virialized, locating itself in the virialized region shown in the left panel. By

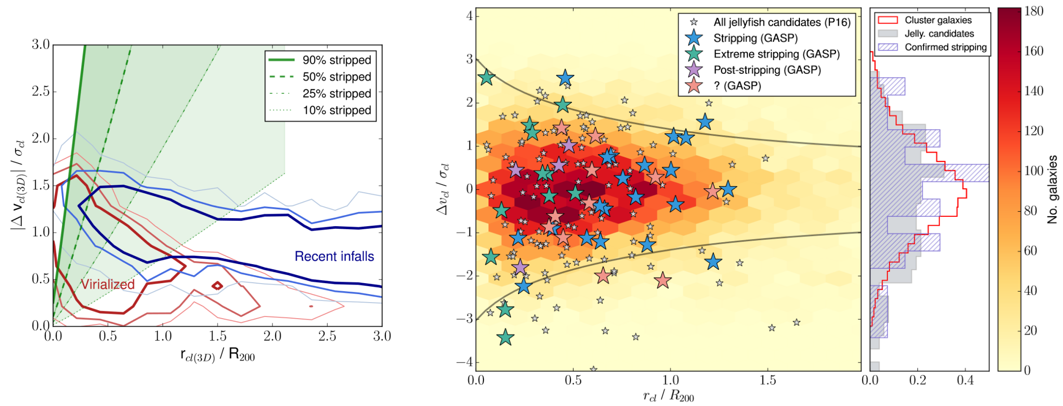

Figure 1.6: Phase-space diagram examples taken from Jaffé et al. (2018). Both diagrams normalize the velocity of the galaxies by the cluster/group velocity dispersion, and the distance to the center by the virial radius R_{200}. Left: Phase-space diagram of 15 simulated group and cluster galaxies from Rhee et al. (2017), separated in virialized and "recent infalls" regions. The green area indicates the region where ram pressure stripping is effective, with varying degrees of stripped fraction which tends to increase as the velocity increases and the distance to the cluster center decreases. Note that the velocity is in absolute value. Right: Line of sight velocity vs. projected position phase-space distribution of jellyfish candidates from P16 (small gray stars) plus a subsample observed with the MUSE instrument by the GASP program (larger colored stars, Poggianti et al. 2017b), with all galaxies from the WINGS and omegaWINGS clusters in the background as a density plot. The gray curve corresponds to the 3D (un-projected) escape velocity in an NFW halo with concentration c = 6 for reference.

this point, we expect the majority of the galaxies to be quenched, as the simulations result in most of the galaxies being completely stripped before their first pericenter passage. If we compare the colors of the galaxies in the virialized region versus the "recent infalls" region, we find redder colors in the former, as well as lower HI contents (Jaffé et al., 2016).

On the right panel of Figure 1.6 we show distributions of jellyfish galaxies and normal galaxies in a projected phase-space diagram, from clusters in the WINGS and omegaWINGS surveys. From here we note that the jellyfish galaxies have a broader velocity distribution when compared to the other cluster galaxies, preferring a high-velocity position in phase-space. This is consistent with jellyfish galaxies being recently accreted into the cluster in radial orbits. Furthermore, extreme cases of ram pressure stripping tend to be near the cluster center and have the largest velocities.

1.3.6 Tail directions of jellyfish galaxies

Another aspect that we can use to constrain the effects of ram pressure stripping, is to take advantage of the tail directions of jellyfish galaxies. Because the tails are expected to point opposite to the direction of motion, we can obtain direct information about the orbits of galaxies with extreme ram pressure stripping. One of the first studies to mention the tail orientation of multiple jellyfish galaxies in a cluster is the work by Chung et al. (2007), where they find that most galaxies with HI tails in the Virgo cluster point away from the cluster center. UV tail directions in the Coma cluster also follow this trend (Smith et al., 2010), and it is further supported by the radio tail distribution found by Roberts & Parker (2020a). This is consistent with a scenario where these galaxies are infalling on mostly radial orbits. Interestingly, merging clusters seem to tell a different story. The merging cluster Abell 2744 does not show the same trend of tails pointing away, where Rawle et al. (2014) finds more perpendicular tails instead. Recent work by Roman-Oliveira et al. (2021) finds no preferred direction in the merging cluster system Abell 901/902. These results could be because of the unrelaxed and complex nature of merging clusters, such that passing shock fronts could have altered the tail direction of the galaxies.

Tail direction studies of optical jellyfish galaxies in multiple clusters began with the large samples that appeared in 2016. On the one hand, P16 provided crude estimations of the fractions of the tail orientations, finding $\sim$ 13% of tails pointing towards, $\sim$ 35% pointing away, and $\sim$ 52% pointing elsewhere. On the other hand, McPartland et al. (2016) made a more extensive study on the direction of motion of their jellyfish candidates, based on the tail directions (although the tail direction distribution is not provided). They used their results in conjunction with hydrodynamical models from Roediger & Brüggen (2006), Kronberger et al. (2008), and Roediger et al. (2014) to constrain the infall histories of the galaxies. They find that their distribution best matches a fast cluster merger scenario, rather than galaxy accretion from filaments or slow cluster mergers. However, their results do not rule out contributions from the other scenarios. Their results also agree with a scenario where jellyfish galaxies might also be observed near the cluster center of low-mass clusters or potentially even in groups.

The recent works of Roberts et al. (2021a) and Roberts et al. (2021b) provide a complete distribution of tail directions from the LOFAR Two-metre Sky Survey (LoTSS) in both clusters and groups, respectively. In the case of clusters, they once again find a distribution that prefers tails pointing away from the cluster center, while in the case of groups, they find a two-peaked distribution, where one peak belongs to tails pointing away (but slightly more perpendicular than in clusters) and another peak belongs to tails pointing towards. A similar two-peaked distribution is found by Kolcu et al. (2022), using tail directions of galaxies in groups from the Galaxy And Mass Assembly survey. These findings could indicate that infalling galaxies in groups experience delayed ram pressure stripping.

A typical general approach used to understand observations is to use cosmological simulations to try to reproduce the same results. However, to reproduce the effects obtained from hydrodynamical mechanisms we need a great understanding of the physics of these processes, and these need to be implemented accurately and with enough resolution in cosmological hydrodynamical simulations. In an attempt to avoid some of these difficulties, a novel semi-analytic approach introduced by Smith et al. (2022) (hereafter S22) was developed to constrain the lifetime of jellyfish galaxy tails. They do this by using N-body cosmological dark matter only simulations, for which they later "paint-on" the galaxy tails using free parameters, which are then constrained by comparing the model with observations using a Markov Chain Monte Carlo (MCMC) model. They apply their method to the LoTSS sample of Roberts et al. (2021a) and Roberts et al. (2021b), using the positions in phase-space plus the tail direction distribution, from which they obtain that radio continuum tails appear on average at ~ 0.76 R_{200}, and disappear on average ~ 480 Myr after pericenter.

1.4 This thesis

The main objective of this thesis is to apply the method from S22 using the direction of tails from a large homogeneous sample of ram pressure stripping candidates to constrain, for the first time, the lifetime of the jellyfish features in the optical regime. Although broad-band optical features only show the tip of the iceberg when it comes to ram pressure stripping, optical images are more accessible, which could allow for larger sample sizes and better statistics. If done correctly, constraining the lifetime of the tails in this wavelength can be useful for modeling ram pressure stripping, as it provides insight into the star formation happening in the tails of jellyfish galaxies. With this work we aim to provide an in-depth study of the directions of optical tails, presenting a methodology that we hope will continue to pave the way for future studies that will take advantage of the continuously growing samples of jellyfish galaxies.

Therefore, the information obtained by this study could also be used to further help future surveys to better search, identify, and classify jellyfish galaxies.

Throughout this thesis we assume a ΛCDM cosmology, with a Hubble constant $H_0 = 70\ \mathrm{km\ s^{-1}\ Mpc^{-1}}$, present matter density of $\Omega_m = 0.27$, and dark energy density $\Omega_\Lambda = 0.73$.

Chapter 2

Data and Method

2.1 Sample and data

In this work, we use the largest homogeneous sample of optically-selected jellyfish galaxy candidates in the low-redshift Universe compiled to date, consisting of 379 galaxies: 344 of them come from the P16 sample, and 35 come from the newly identified candidates from Vulcani et al. (2022) (hereafter V22). Both of these samples were visually selected from broad-band optical images of clusters from the WINGS and omegaWINGS surveys (Fasano et al. 2006, Gullieuszik et al. 2015). In short, WINGS is a survey of 77 low redshift ($z \sim 0.04 - 0.07$) galaxy clusters selected on the basis of their X-ray luminosity (Ebeling et al. 1996, 1998, 2000). The WINGS data consists of B and V band photometry plus spectroscopy for most of the clusters, with a typical field of view of $34' \times 34'$, which translates into an average coverage of ~ 0.8 R_{200}. OmegaWINGS is an extension of WINGS that quadruples the field of view for 46 of the clusters, yielding an average coverage of ~ 1.2 R_{200} for this sub-sample.

In the original jellyfish candidate sample from P16 searched for ram pressure stripping features such as unilateral debris or tails in the optical images. Up to three classifiers assigned to each jellyfish candidate a "Jellyfish Class" (JClass), which is a visual indication of the strength of the stripping features, going from extreme cases (JClass = 5) to progressively weaker cases, with the weakest case being JClass = 1. The new candidates from V22 are missed galaxies from P16, after a re-inspection of the clusters using the same criteria. It is important to note that while P16 inspected all cluster galaxies (in the photometric sample), V22 only considered spectroscopically confirmed members.

To minimize the noise in our results, for the present work, we have further cleaned the sample of jellyfish galaxy candidates from possible tidal interactions. We did this by considering the comments in table 3 from P16 and flagged 66 galaxies with indications of tidal interaction or merger. We also cleaned the sample of clusters from highly interacting clusters. To this end, we used the classifications of the cluster dynamical states described in Lourenco et al. (submitted), for which we consider interacting clusters those flagged as pre-merger, interacting, and post-merger. This yielded 9 interacting clusters (containing 46 jellyfish candidates in total). Lastly, we removed 76 jellyfish candidates that are confirmed non-members. After filtering the data we are left with a clean sample of 227 jellyfish galaxy candidates.

We note that our sample of jellyfish candidates includes 11 unwinding galaxies identified by Bellhouse et al. (2021). These are galaxies that have unwinding-spiral arms likely due to ram-pressure stripping viewed close to face-on. The connection between ram pressure stripping and unwinding spiral arms is yet to be fully understood (see V22) so we exclude these galaxies from part of our analysis (as indicated) when their potential uncertainty could significantly affect the results. We also note that while V22 also provides a large sample of newly-identified unwinding galaxies (from which some might be ram pressure stripped), we do not consider them in our analysis.

In what follows we use stellar masses (M_*) and redshifts from V22. B and V absolute magnitudes for most of the WINGS and OmegaWINGS galaxies (also including non-jellyfish candidates, which we use for reference) were taken from Varela et al. (2009).

Cluster properties (including velocity dispersion, σ_{cl}; sizes, R_{200}; and host mass, M_{200}) come from Lourenco et al. (submitted) and Biviano et al. (2017). Cluster memberships are also taken from Lourenco et al. (submitted) which uses the method described in Biviano et al. (2017), based on projected position-velocity phase-space. In our parent sample of jellyfish candidates, we have 195 confirmed members, 76 confirmed non-members, and 108 candidates with unknown redshift. Finally, the corresponding BCG for each cluster is taken from the BCG sample in Fasano et al. (2010), which we treat as the cluster center.

2.2 Measuring the tail directions of jellyfish galaxies

We use the optical images of our jellyfish galaxy sample to measure the direction of the tails relative to the center of the clusters. To robustly determine this tail angle for each galaxy, up to seven classifiers inspected the galaxies and interactively drew the tail directions through the use of a custom-made Python script, which allows the classifiers to directly draw the projected tail direction on top of an optical image. To maximize the visibility of the (often) low-surface brightness tails, we selected six different logarithmic min-max scales of the B-band WINGS/omegaWINGS images to provide a wide range of views to choose from to determine tail directions. We also used RGB images from the Legacy Survey (Dey et al., 2019) for the galaxies, when available. Lastly, the classifiers could choose to add contours to the image or zoom in/out if they deemed useful (see example in Figure 2.1). Each classifier would also assign a confidence level based on the clarity of the tails, with possible values of 0, 1, or 2; these being no tail, marginal tail, or clear tail, respectively. When a classifier finishes drawing the tail, the direction is computed as the angle with respect to the x-axis of the images from Figure 2.1 in a counterclockwise manner.

For an initial inspection of the agreement of the results between the classifiers, we compared the difference in the angles measured between different pairs of classifiers, as shown in Figure 2.2. Although not all comparisons are shown in the Figure, in general, we find that the classifiers tend to agree remarkably well with each other, with the majority of the measures agreeing within a margin of 45 degrees. We also note that measures with a difference greater than 45 degrees are relatively few in number. We can further remove some of these clear outliers by following the flowchart from Figure 2.3, which effectively removes a significant percentage of them.

To further quantify the agreement in the classifications, we computed the scatter of the angles obtained for each galaxy that had at least 2 classifiers with a confidence level greater than 0 (i.e. with a visible tail). For this, we used the definition of the standard deviation given by

$$\sigma_{\text{angle}} = \sqrt{\frac{\sum (\Delta\theta_i)^2}{N}}, \tag{2.1}$$

where N is the number of classifiers, and $\Delta\theta_i$ is given by

$$\Delta\theta_i = \begin{cases} \mid \theta_i - \overline{\theta} \mid, & \text{if } \mid \theta_i - \overline{\theta} \mid \leq 180^{\text{o}} \\ 360^{\text{o}} - \mid \theta_i - \overline{\theta} \mid, & \text{otherwise} \end{cases} \tag{2.2}$$

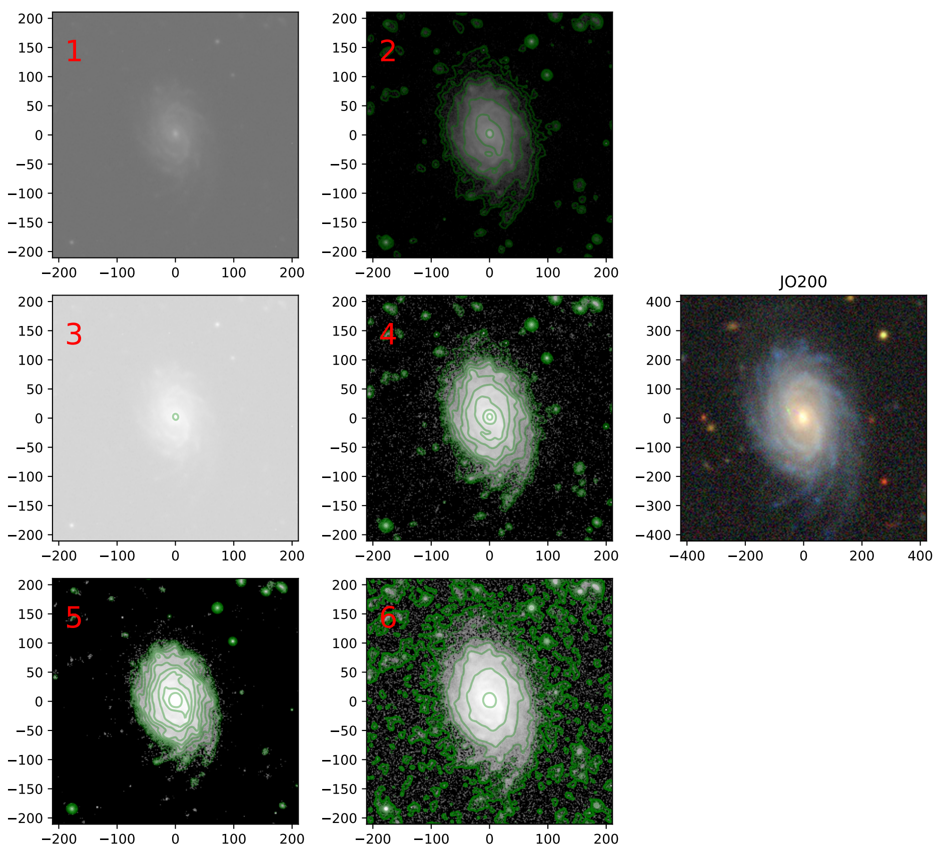

Figure 2.1: Example of the images used for classification of the tail directions. All images are oriented with the north pointing up and the east pointing to the left. The numbered images are B-band images taken from P16 using different scales, with contours plotted on top. The image on the right is an RGB image taken from the Legacy Survey. Each classifier was able to inspect and then choose any combination of image and contours (or only an image without contours) to determine the tail direction.

where θ_i is the angle obtained by the ith classifier, and $\overline{\theta}$ is the circular average of the angles given by the N classifiers. Note that we are using the circular average and this definition of $\Delta\theta_i$ to account for the fact that angles are cyclic quantities. The distribution of standard deviations is presented in Figure 2.4, where we find an average standard deviation of ~ 32 degrees.

The final tail angle for each galaxy is computed as the circular average from the results of all classifiers that agreed in the direction of the tail with a difference no greater than 45 degrees. We use 45 degrees as a boundary in angle differences to detect outliers in the tail direction measurements, which is slightly larger than the average scat-

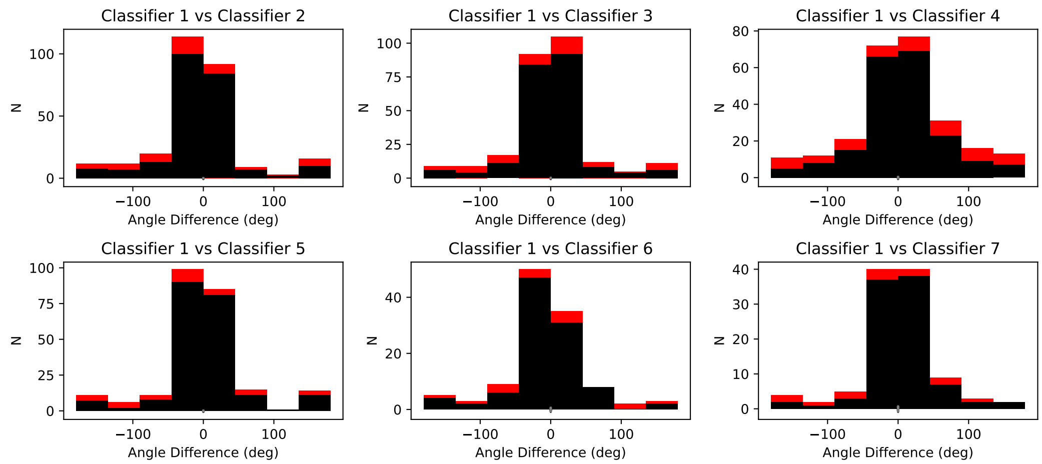

Figure 2.2: Distribution of tail angle differences between the different classifiers. Each subplot includes a red histogram representing the distribution of the difference in the tail angle with respect to classifier 1, which includes all the galaxies where both classifiers agree to see a tail. The black histograms are the same as the red ones, but excluding the measurements rejected by the flowchart from Figure 2.3. All histograms have a bin size of 45 degrees. Note that most of the galaxies are concentrated within -45 and 45 degrees, which is true even if we consider the unfiltered red histograms.

ter obtained (see vertical lines in Figure 2.4). The process of obtaining an average tail angle followed the flowchart from Figure 2.3, which is based on the work by Kolcu et al. (2022) (modifications were made to the angle rejection criteria to better suit a larger number of classifiers), and guarantees that the majority of the classifiers need to agree to see a tail (confidence level greater than 0), and that the majority unanimously agrees on a particular direction. Otherwise, the galaxy is classified as a jellyfish candidate with no tail. The final confidence level assigned to galaxies with tails is taken as the one with the higher number of votes. If a galaxy has an equal number of votes for marginal or clear tail, then we assign a marginal level for that galaxy.

In Figure 2.5 we present 6 randomly-selected example galaxies with the tail directions of each classifier drawn on top as colorful arrows and the average tail direction (after flowchart procedure) in a bigger white arrow. In the appendix, we present a diagram with the resulting tail directions and galaxy positions with respect to the BCG (Figure A.1), and a full display of the images with the tail directions measured by all classifiers is available in Figure A.2.

After computing the mean tail angles with respect to the x-axis we transformed

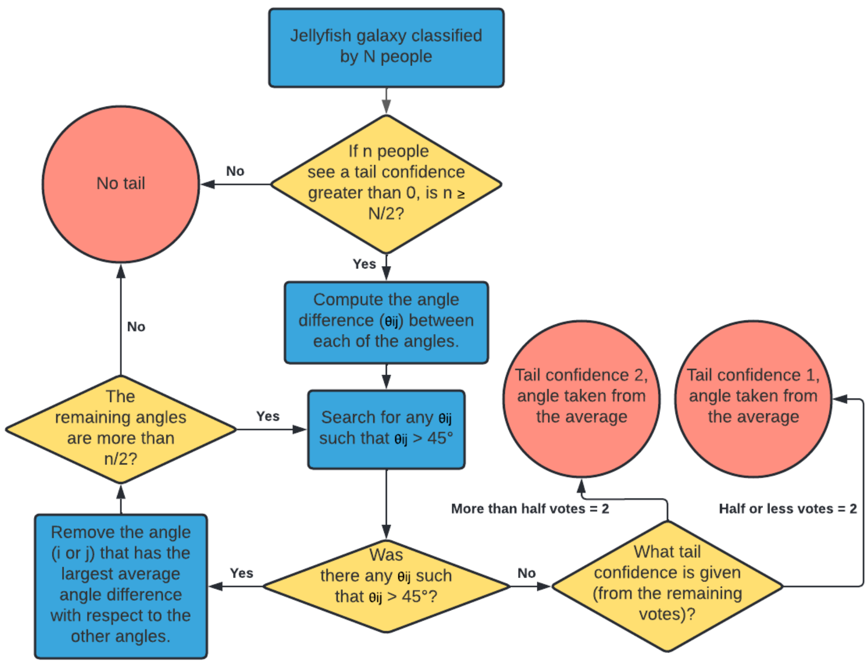

Figure 2.3: Flowchart followed to determine the mean tail angles of the stripped galaxies and the associated confidence of the measurement.

them into angles of the tails relative to the direction of the BCG, following the same convention used by S22 and Kolcu et al. (2022), such that angles close to 0 degrees would indicate tails pointing towards the BCG, while angles close to 180 degrees would indicate tails pointing away from the BCG (see Figure 2.6). In this work, we will refer to this angle as the tail-BCG angle. Table A.1 in the appendix provides the tail angle results for each candidate.

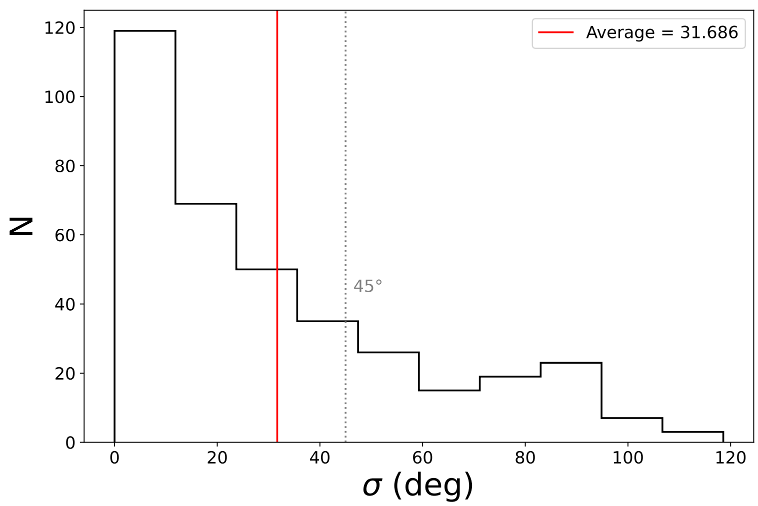

Figure 2.4: Standard deviation distribution of tail angles for galaxies in which more than one classifier agrees to see a tail. Note that this result serves as an initial test on the agreement of the classifiers, therefore it is not applying the flowchart procedure described in Figure 2.3.

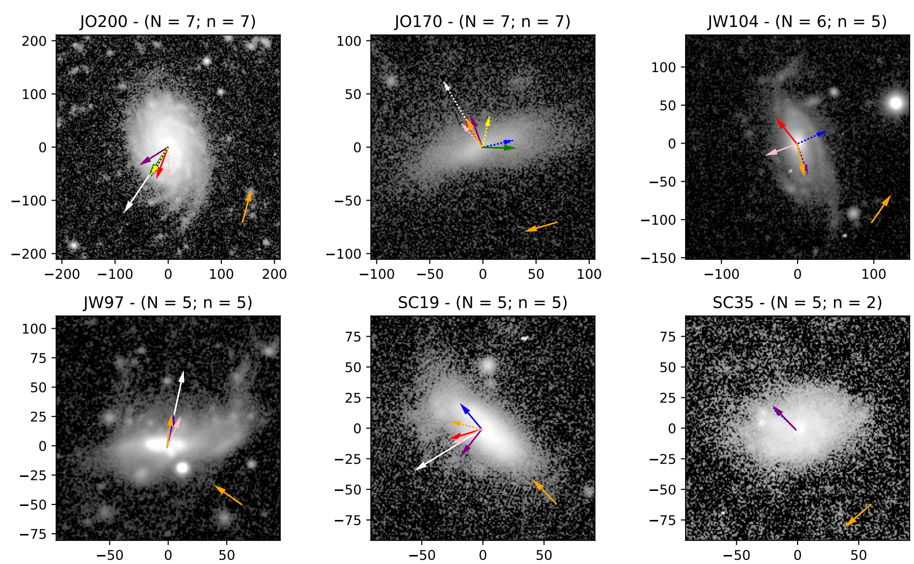

Figure 2.5: Example of images with arrows representing the tail directions of each classifier and the resulting mean tail when applying the flowchart of Figure 2.3. The short colored arrows at the center of each image represent different classifiers, while the larger white arrows represent the mean angle. Clear tails are represented with a solid line and marginal tails with a dotted line. The orange arrows at the bottom right corner point in the direction of the BCG. The subtitles indicate the name of the galaxy, the number of classifiers (N), and the number of classifiers that see a tail (n).

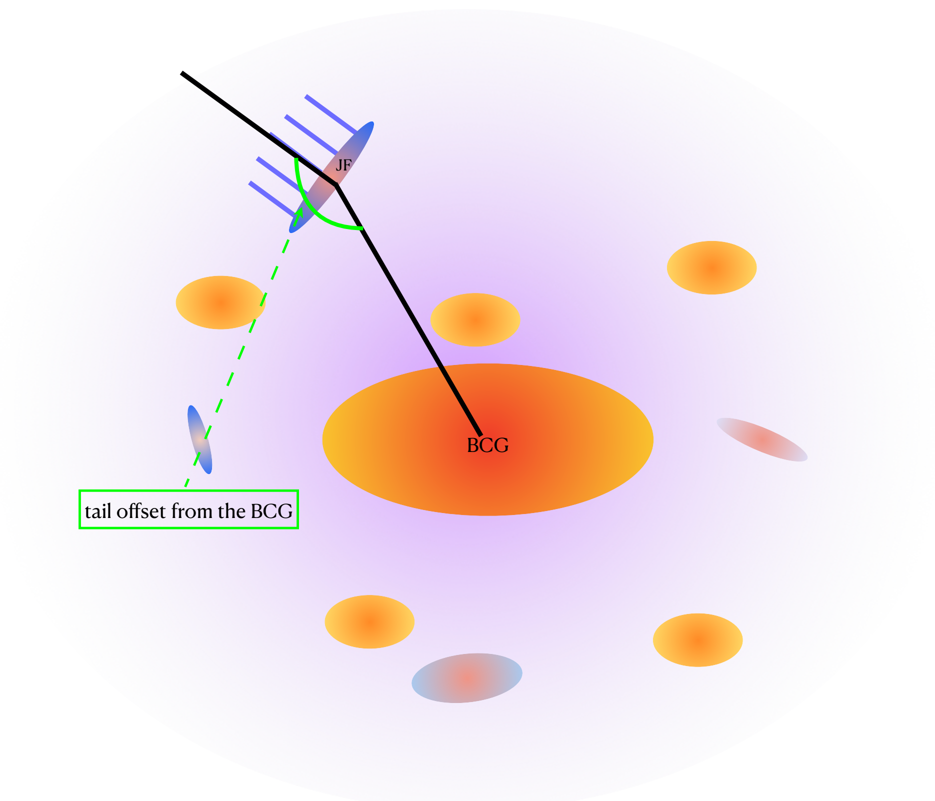

Figure 2.6: Tail angle diagram. The green angle represents the angle of the tail with respect to the direction of the BCG (tail-BCG angle). The angle can range between 0 to 180 degrees. Diagram credited to Jacob Crossett.

CHAPTER 3

Results

3.1 Comparison with Hα

To test how reliable are our tail measurements based in broad-band optical images, we compared them with tail measurements done on Hα maps from the GASP survey (Poggianti et al., 2017b), which is a MUSE program targeting stripped galaxies from P16. Since Hα emission usually provides a clearer tracer of the tails than broad-band optical images, comparing our results with tail directions using Hα provides a good way of estimating the accuracy of the results. For this comparison, we are using a subsample of 47 galaxies observed by GASP and inspected for tail directions. The tail directions for these Hα maps were visually measured based on the asymmetry of the Hα emission with respect to stellar contours.

The classification of the GASP images gives 41 galaxies with confirmed tails in Hα, out of which 35 also have visible tails in the optical. Note that this difference could be due to faint Hα tails not being easily detected in broad-band optical images. However, when tails are seen in both wavelengths we would expect to obtain similar tail directions, such that any deviation can then be interpreted as a systematic error arising from our methodology, which could be caused by the increased difficulty of accurately classifying broad-band optical tails. Figure 3.1 presents optical images of the galaxies for which the optical (blue) and Hα (yellow) tail directions were compared. The quantified discrepancies are further shown in the diagram of Figure 3.2, where it is clear that there is a good agreement overall, finding that 30% of the galaxies have a discrepancy greater than 45 degrees, which translates into an agreement of 70%. Furthermore, the circular average of the discrepancy gives -4.2 degrees (very close to 0 degrees), with a standard deviation of 55.9 degrees following Equation 2.1.

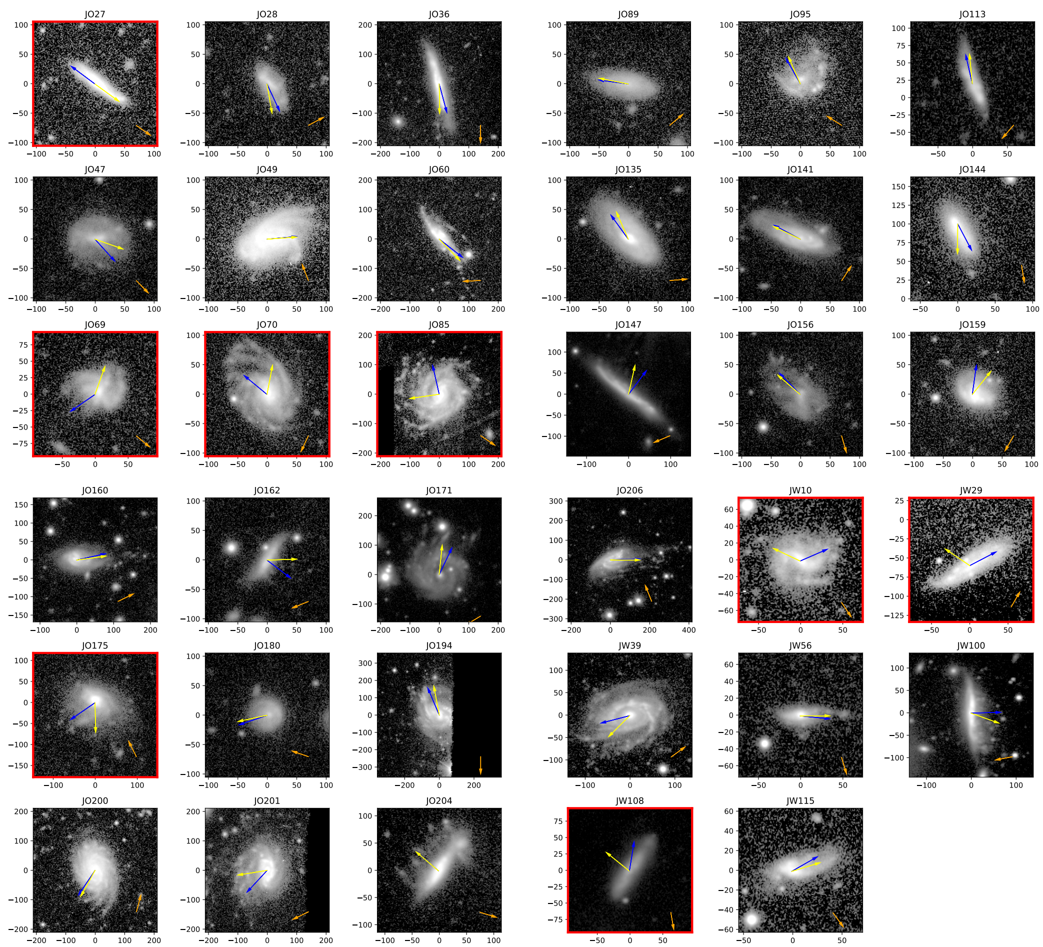

Figure 3.1: B-band images from WINGS/omegaWINGS of the 35 galaxies with tails in both optical and Hα emission, with arrows representing the tail directions in the optical (blue arrows) and in Hα (yellow arrows). The orange arrow at the bottom right corner points in the direction of the BCG. Images with red axes highlight cases where tail measurements have a difference greater than 45 degrees.

When inspecting the 8 galaxies with large tail angle discrepancies, we find that 4 of them are unwinding galaxies, which likely relates to a higher difficulty in accurately classifying the tails of these galaxies when compared with the other cases. Interestingly, all unwinding galaxies in this subsample have confidence = 2, suggesting the

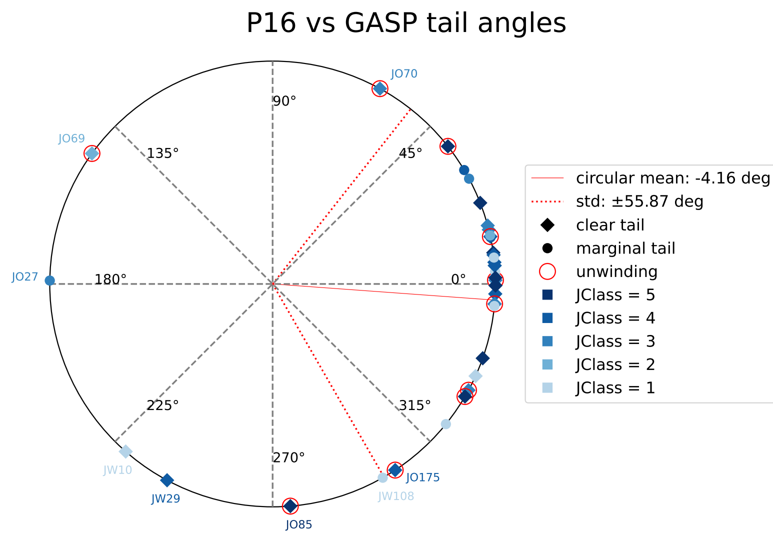

Figure 3.2: Optical vs. H*α* tail angles. The points in the plot represent the difference between the optical tail angles in this work and H*α* tail angles in a subsample from the GASP project (Poggianti et al., 2017b). Clear tails are represented by diamonds and marginal tails are represented by circles. Galaxies with unwinding spiral arms are encircled in red. Note that 8 out of 35 measurements have a larger discrepancy than the expected error of 45°, where half are unwinding galaxies.

tails were clear. This indicates that unwinding galaxies usually show clear signs of the existence of a tail, but that the correct tail direction is trickier to determine, possibly because it involves some degree of extrapolation, since the apparent tails may not always point directly opposite to the direction of motion because of disk rotation. Additionally, these galaxies can only be observed face-on, which could further complicate their tail measurement. The other 4 galaxies that are not unwinding require individual reasons for the discrepancy. In the case of JW10, JW29, and JW108, the difference is caused due to the clear amount of the observable debris in the H*α* maps, which are not as easily observed (or not observed at all) in the optical broad-band images. However, in the case of JO27, which has the largest discrepancy with each arrow pointing in the opposite direction of one another, we do not particularly find a clear indicator of the tail direction from the H*α* emission, nor from the optical image (classified with marginal confidence). An argument could be made for either of the two directions or even for the non-existence of a tail. Therefore, this is a rare example where a discrepancy with H*α* does not necessarily means the optical tail direction is wrong.

In conclusion, when comparing broad-band optical versus Hα measurement of tail direction in jellyfish candidates, we find that, although tails are more clearly visible through their ionized gas, there is a good agreement. This test serves as support and provides confidence to optical studies such as the present one.

3.2 Tail angle distribution

3.2.1 Overall tail angle distribution

From the tail classifications, we find that 71% of the jellyfish candidates have tails in both the unfiltered and clean samples. Clear tails are found in 28% of the cases (39% if we consider only galaxies with tails). Figure 3.3 shows that the overall distribution of the jellyfish tail-BCG angles is dominated by galaxies with high angles, which indicates their tails are pointing away from the cluster center. This is consistent with ram pressure stripping being stronger for galaxies following radial orbits on first infall. Previous tail directions studies in various wavelengths (e.g. Chung et al. 2007, Smith et al. 2010, Roberts & Parker 2020b, Roberts et al. 2021a) obtain similar trends.

In this work, we define 3 categories of tails depending on their orientation: ”towards”, ”perpendicular”, and ”away” from the cluster center, corresponding to galaxies within the first, second + third, and fourth bin of Figure 3.3 (from left to right) respectively. Note that the notation used in these classifications refers to the tail direction relative to the cluster center, which is usually opposite to the direction of motion. Using these definitions and considering the clean sample (excluding confirmed non-members, interacting clusters, and interacting galaxies) we find fractions of 18.5% towards, 48.8% perpendicular, and 32.7% away. This is mostly consistent with the original P16 estimates, as the only sample with a (slightly) significant difference when compared to the respective error bars are the galaxies pointing towards the cluster center, which increased by 5.5%.

Contrary to the distributions in Figure 3.3, in Figure 3.4 we plot the distribution of tail directions only within interacting clusters, obtaining a much flatter distribution instead. This justifies their exclusion from the clean sample and suggests that galaxies within unrelaxed clusters might be subject to particular conditions that alter the orbits of the galaxies and/or the medium surrounding them, which could have an effect on both the effectiveness of ram pressure stripping and in the direction of the tails. If we filter by tail confidence we find a more similar distribution to the non-interacting sam-

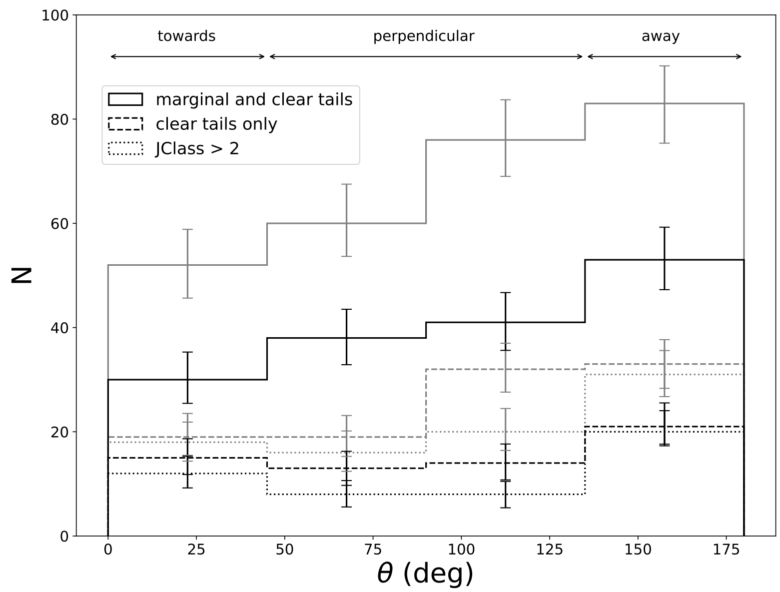

Figure 3.3: Tail-BCG angle distributions. The gray histograms are including the full parent sample, and black histograms are excluding interacting galaxies, galaxies within cluster mergers, and confirmed non-member galaxies. Histograms with solid lines represent all galaxies with tails in the respective sample, dashed lines only include galaxies with clear tails, and dotted lines only include galaxies with JClass greater than 2. Error bars were computed as the standard deviation from bootstrapping resampling.

ple, although not entirely since we find a peak at a lower angle (third bin) than in the clean sample. However, in general, higher angles remain preferred. This indicates that galaxies with clear tails within unrelaxed clusters remain preferentially found in cases where the galaxy is moving towards the cluster center, but likely with fewer cases of radial orbits than in relaxed clusters. More perpendicular orbits likely experience less effective ram pressure stripping, preferentially producing marginal tails, hence why the clear tail distribution is less normalized. The tail distribution for high JClass candidates is only slightly different from the clear tail distribution, although the statistics are very poor, showing relatively large error bars and a small sample size. While tail clarity and JClass (which measure signatures of ram pressure stripping) are different criteria, we expect them to be related to some extent. However, the complex nature of unrelaxed clusters could potentially introduce some differences in both filter criteria. Possible factors that could enhance or suppress ram pressure stripping signatures are passing shock fronts (Rawle et al., 2014), which could alter the velocities of galaxies relative to the medium and/or the density of the medium by moving the material

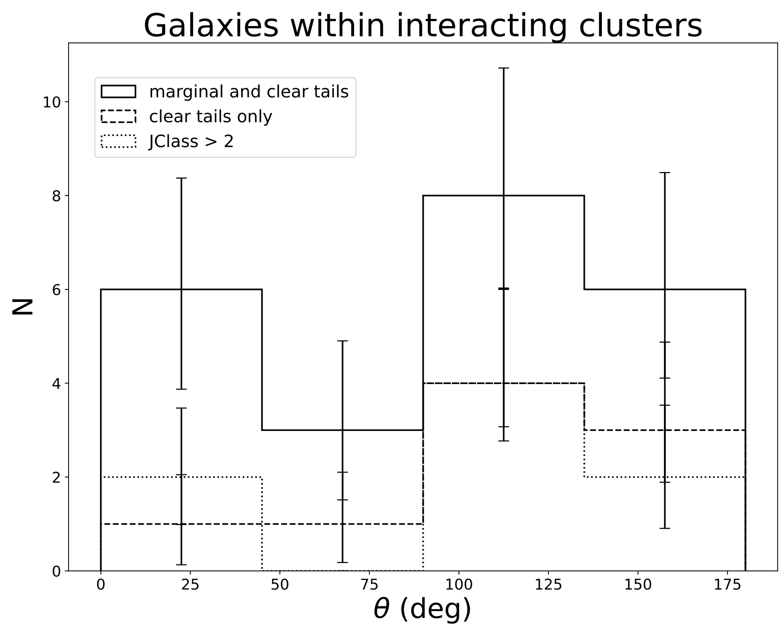

Figure 3.4: Jellyfish tail angle distribution for galaxies within interacting clusters. This sample is excluding confirmed non-members and interacting galaxies. Histograms with solid lines represent all galaxies with tails in the sample, dashed lines only include galaxies with clear tails, and dotted lines only include galaxies with JClass greater than 2. Error bars were computed using bootstrapping.

farther or closer to the galaxies. Unfortunately, with the limited sample we have for candidates in interacting clusters, we can only provide speculative interpretations. Better statistics and a more detailed analysis would be needed to have a good understanding of the effect of interacting clusters on galaxy tails since their properties could widely vary for different interacting clusters. The work by Piraino et al. (submitted) will provide a jellyfish tail study of galaxies in the unrelaxed cluster A2670, adding further insight into these types of environments.

Another interesting result seen in Figure 3.3 is obtained from the tail distributions when only using galaxies with JClass > 2 or clear tails only (dotted and dashed histograms), having very similar overall distributions. Instead of finding a monotonically increasing number of galaxies as we move from the first to the last bin, we find a second peak for galaxies pointing towards the cluster center and a lower fraction of perpendicular tails. This type of distribution is not only observed in this case, but also in the distribution of the Hα tail directions. This result indicates that, as expected, the clearest and most extreme cases of ram pressure stripping do not have perpendicular tails. Instead, a significant number of galaxies with tails pointing towards the cluster center becomes apparent. These would be galaxies in radial orbits that have passed pericenter and are moving away from the BCG. There are two possible interpretations for this result; the simplest one would be a projection effect, such that enough tails pointing away from the BCG appear as if pointing towards the BCG, therefore producing the second peak. Given the size of the subsample, this is plausible since the error bars of the perpendicular sample are within the range shown by the error of the towards sample, and perhaps with a larger sample we could find a different result. The other possibility would be that this fraction is accurate to reality (with some contamination expected from projection effects), in which case this result would be indicating that examples of extreme cases of on-going ram pressure stripping can also be significant even after the first pericenter passage. This would mean that not all galaxies are completely stripped on first infall, and that ram pressure stripping can remain effective in producing tails after pericentric passage.

Because the fraction of towards cases is the smallest in the full sample, despite being significant when considering the distributions of high JClass or clear tails only, confirms that outfalling galaxies with optical tails are not common occurrences when compared with perpendicular orbits, and especially with respect to infalling ones. Therefore, a significant number of infalling galaxies should indeed stop having visible tails before or shortly after reaching pericenter. Then, the lack of visible tails pointing towards can be caused by a combination of scenarios; cases where the initially radial orbits have turned into circular orbits (joining the perpendicular sample), cases where the gas content is completely stripped before or shortly after pericenter passage, and cases where ram pressure becomes too weak for effective stripping because of the expected loss of velocity and progressively less dense medium as the galaxies move away from the cluster center. However, the latter scenario seems disfavoured (although most likely a contributing factor) by the finding of the second peak in the first bin when considering the most extreme examples of ram pressure stripping.

In an attempt to further test the hypothesis that not only galaxies with high tail-BCG angles (infalling) experience high ram pressure stripping, but that galaxies with low tail-BCG angles (presumably outfalling) can also be experiencing significant stripping, in Figure 3.5 we present the JClass distributions for the (clean) subsamples of tails pointing away, towards, and perpendicular to the cluster center. From here we find that $\sim 40\%$ of the galaxies in both the towards and away samples have a JClass > 2, which is twice the fraction of JClass > 2 galaxies in the perpendicular sample.

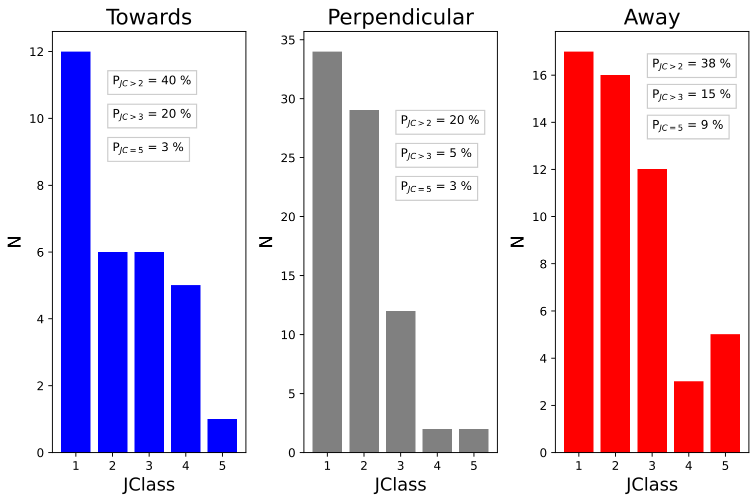

Figure 3.5: Number of galaxies on each JClass, for each tail-BCG angle sample from the histogram in Figure 3.3. JClass goes from extreme cases (JClass 5) to progressively weaker cases, down to JClass 1. The distributions are excluding confirmed non-members, interacting galaxies, and interacting clusters.

If we are more conservative with our definition of high JClass, we find that only 5% of the perpendicular tails have JClass $>$ 3, while 20% and 15% have JClass $>$ 3 in the towards and away sample, respectively. Interestingly, we find a higher percentage of high JClass candidates in the towards distribution than the away sample, but it is dominated by JClass 4 galaxies, with only 3% of them having a JClass 5 classification. In contrast, the away sample has a 9% of JClass 5 galaxies. These results are indicative that the most extreme cases of ram pressure stripping still come from infalling galaxies on radial orbits, but that the stripping features can be often visible past pericenter since the towards galaxies have signatures of stripping almost as significant as the away ones.

3.2.2 Tail angle distribution for different coverages

So far we have presented the tail distributions using all jellyfish candidates from WINGS and omegaWINGS combined, using candidates from both P16 and V22. However, not all clusters have the same observational coverage as they vary in mass, redshift, and also not all WINGS clusters were observed by omegaWINGS, which had a significantly wider field of view. So in order to fairly combine the tail measurement results of different clusters we limit the sample to clusters that have observations covering up to a given minimum radius $r_{\min}$ and only consider galaxies within a circular aperture of this radius. Ideally, we would like $r_{\min}$ to be larger than R_{200} but when imposing this constraint the sample decreases significantly. We therefore consider in our analysis 3 values for $r_{\min}$: 0.7, 1 and $1.2R_{200}$.

In Figure 3.6 we show the jellyfish galaxy tail angle distribution for the different $r_{\min}$. On the left panels, we have further excluded galaxies that are not confirmed cluster members as indicated by their redshift. In this case, we have included the sample of new stripping candidates from V22. The right-hand side of the plot shows the same distribution considering all galaxies (many of which do not have redshifts), but candidates from V22 are not included. We removed them because this jellyfish candidate sample was constructed from a parent sample with confirmed members (unlike P16) and we wanted to construct fair samples, trying to avoid potential biases. However, if we include the V22 candidates the distributions have minimal changes, maintaining the same general shape on every panel.

For $r < 0.7R_{200}$ (upper panels in Figure 3.6) we obtain a qualitatively similar distribution to the one in Figure 3.3 for JClass > 2 and clear tails (dotted and dashed histograms), where the tail directions are dominated by high angles, but showing a second peak for tails pointing towards. In this case, we find this type of distribution regardless of tail clarity, JClass, or confirmed membership. Therefore, applying this cut appears to trace a somewhat similar distribution to filtering by high-confidence jellyfish galaxies, albeit not excluding as many galaxies with perpendicular tails. This would be consistent with the idea of ram pressure being stronger near the center.

For $r < 1R_{200}$ (middle panels in Figure 3.6) the distribution does not show a second peak like in the upper panels, instead being similar to the complete distribution of Figure 3.3 (solid histogram). An advantage of the middle panels is that we do not expect a bias (caused by the exclusion of tail orientations preferentially found farther from the center) to have a large impact on the distribution. This is because the work of S22 suggest radio continuum tails form on average at $\sim 0.76R_{200}$, and we do not expect optical tails to have a significantly larger average clustercentric distance when they first become visible than radio tails. Although, many outliers are expected and even observed in this sample (see Figure A.1 in the appendix). Note however that the sample size reduced significantly for this sample compared to the upper panels.

For $r < 1.2R_{200}$ (bottom panels in Figure 3.6) there are even fewer galaxies because many cluster coverages do not reach far enough, which is unfortunate because this subsample should have the least amount of biases, and does not make the assump-

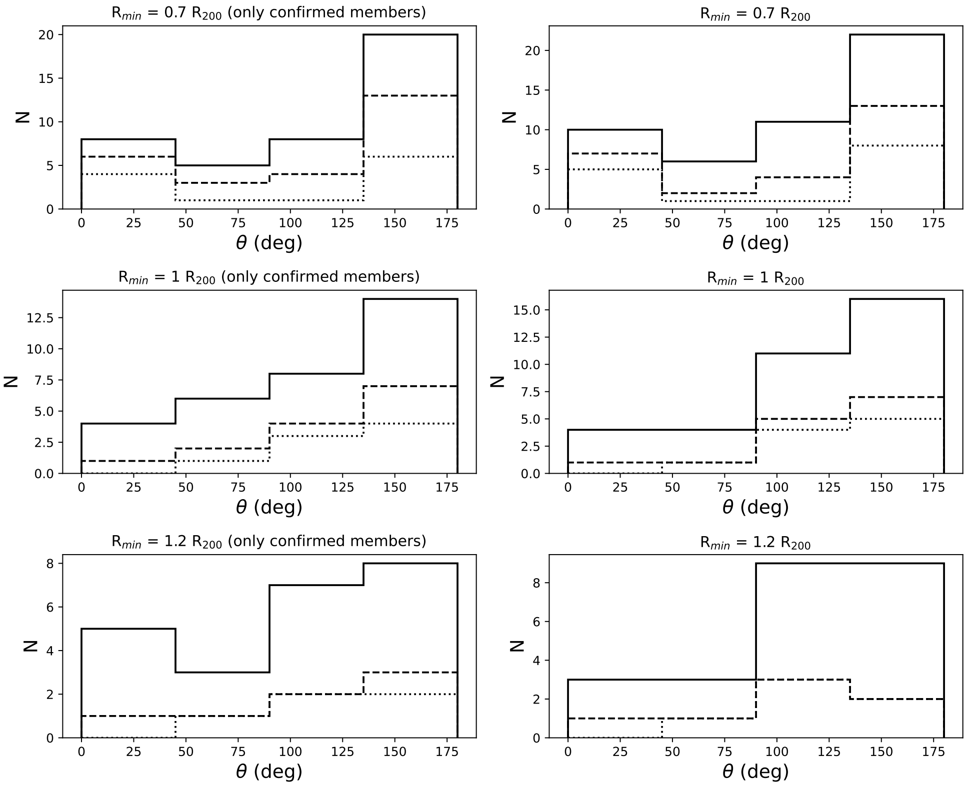

Figure 3.6: Jellyfish tail angles for different $r_{\rm min}$ (top: $0.7R_{200}$; middle: $1R_{200}$; bottom: $1.2R_{200}$). On the left side we only consider confirmed cluster members and in this case, include P16 galaxies and new stripping candidates from V22. On the right-hand side, we only plot stripping candidates from P16 and ignore spectroscopic membership. Error bars for each bin were omitted to not overcrowd the plots, however, they have typical sizes that range between ± 1 and ± 3.5 (computed via bootstrapping). All plots exclude confirmed non-members, gravitationally interacting galaxies, and galaxies in interacting clusters.

tion that optical tails appear on average below $1R_{200}$. From here we once again find a distribution dominated by high tail-BCG angles, but in this case, the left and right panels have more noticeable differences, probably due to low-number statistics. Surprisingly, the second peak in the first bin reappears in the bottom left panel. However, because of the sample size, we should be wary of projection effects. Two out of five galaxies within this bin have larger clustercentric distances than $1R_{200}$, which is odd for galaxies pointing towards the cluster center. Furthermore, both have a marginal tail classification and the clear tail and high JClass distributions do not show this peak, which puts in question whether this result can be trusted, especially in such a small-sized sample where the statistical error is around ± 2. In another respect, a minor difference is present when comparing the high tail confidence distributions (dashed or dotted histograms). The one on the right has a lower fraction of tails pointing away from the BCG, which might suggest that at these distances some galaxies may not be as strongly bound to the cluster potential well. However, with such poor statistics (error bars around ± 1) it is tough to pull an accurate conclusion out of these results.

In summary, Figure 3.6 shows that the tail angle distribution is always shifted towards high angles (i.e. galaxies with tails pointing away from the cluster center), and a secondary peak at low angles is visible at the inner region of the cluster. This could be due to the fact that tails do not last for a long time after pericenter. Another interesting result is the higher fraction of perpendicular tails in the outer region of the clusters, where non-radial orbits can be more easily seen.

3.3 Phase-space distribution

Besides the tail angle distributions, we can use the locations of jellyfish galaxies in a projected velocity vs. clustercentric distance phase-space diagram as an additional observational constraint. In Figure 3.7 we show the phase-space diagram (left panel) for the subsample of 191 confirmed members, distinguishing between tail confidence and tail orientations using different colors.

If we inspect the locations of the tail orientations in phase-space, it is interesting to note that tails pointing away cover a wide range of velocities and clustercentric distance, with a high concentration of them being found around $\sim 0.5R_{200}$ (but see section 3.4 for a more complete description of the radial distribution). Similarly, perpendicular tails peak at this same value and cover slightly larger distances, but with lower velocities. In contrast, the towards sample is less concentrated in the bottom left region which is where virialized galaxies dominate. Another empty area for the towards sample can be seen around the upper right region, between ~ 0.6 and $\sim 1R_{200}$. However, a few low confidence tails pointing towards can be seen at clustercentric distances larger than $1R_{200}$, even more so than tails pointing away. However, it is hard to believe these are real cases of radially outfalling galaxies whose tails survived up until that point, especially considering the lack of examples in between. Further inspection of these galaxies might be necessary.

Following S22, we divide the phase-space diagram at $r/R_{200} = 0.5$ and $v/\sigma = 1$, into four regions (labeled A, B, C, D in Figure 3.7), and in Figure 3.8 we present the jellyfish candidate counts on each region. In the upper left region (A) of phase-space,

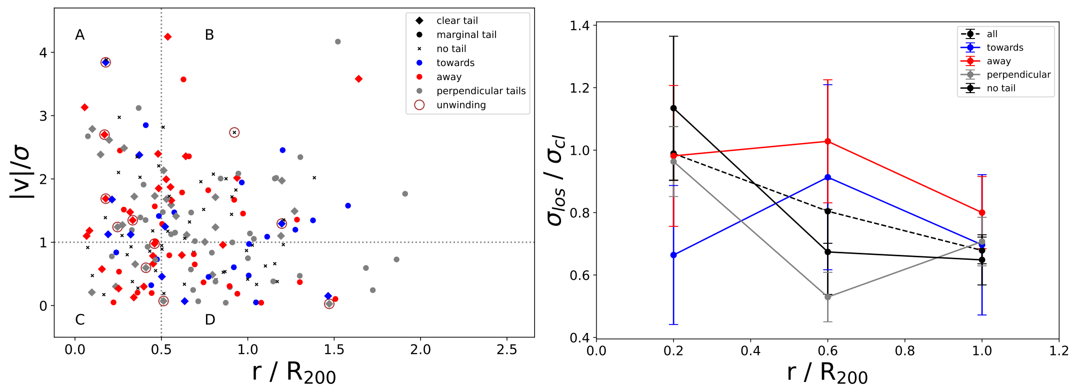

Figure 3.7: Left: Projected phase-space diagram for all spectroscopically confirmed members. This plot does not include interacting galaxies, or galaxies coming from interacting clusters. We highlight tails pointing towards (blue) and away (red) from the BCG, as well as those with perpendicular (gray) tails and no tails (black). Right: Normalized line of sight velocity dispersion radial profiles for the galaxies on the phase-space diagram, but excluding unwinding galaxies. We show the radial profile for all confirmed members (dashed black), as well as the subsamples of galaxies with no tail (solid black), galaxies with tails pointing towards (blue), away (red), and perpendicular (gray) to the BCG. The velocity dispersions are computed as the jackknife standard deviation of the y-coordinates from the phase-space diagram, within radial intervals of width 0.4 R_{200}. The error bars represent the error of the standard deviation obtained by the jackknife method.

where we expect RPS to be the strongest (see Jaffé et al., 2018), we find that 65% of the galaxies with tails have a high confidence classification. This represents the highest fraction of clear tails. The second highest fraction of clear tails is in the lower left region (C) with 52%, followed by the upper right region (B, 39%) and the lower right region (D, 22%). This is consistent with ram pressure starting when the galaxies enter the cluster (at high radii and low velocities), and developing stronger signatures of stripping as they approach the cluster core, especially those with high velocities.

In the right panel of Figure 3.7 we further show the radial profile of the velocity dispersion for all the jellyfish galaxies in the phase-space sample, except for unwinding galaxies. We exclude unwinding galaxies from the velocity dispersion profile (VDP) because unwinding galaxies proved to be the trickiest galaxies to accurately determine the tail direction, and the unwinding feature in clusters has not yet been confirmed to be exclusively linked to ram pressure stripping. We calculate the velocity dispersion using the jackknife method. Note that error bars are large due to the low number statistics of the sample in each bin, which should be taken into consideration when

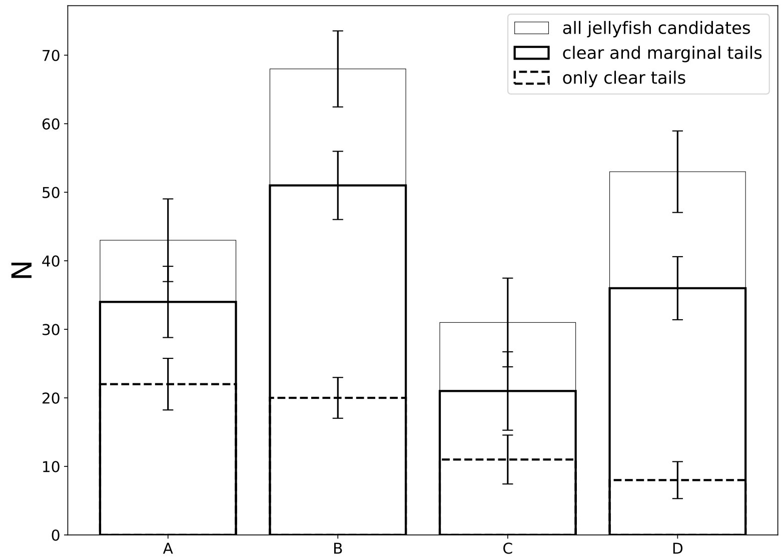

Figure 3.8: Number of jellyfish candidates on each region (A, B, C, D) from the phase-space diagram in the left panel of Figure 3.7. Bars with a narrower solid line represent candidates with any tail confidence (including no tail), while the bars with thicker lines only include candidates with tails. Dashed bars only include galaxies with clear tails. Error bars were computed using bootstrapping.

analyzing this result.

We find that galaxies pointing away have higher velocity dispersions at all radii when compared with the perpendicular and towards tails. Perpendicular tails have a similar dispersion to the away sample near the cluster center but have the lowest overall VDP. This is consistent with galaxies with tails pointing away and towards having very radial orbits, but perpendicular tails being less radial. However, it should be noted that finding as high of a dispersion of perpendicular tails only near the cluster center is not completely unexpected, because galaxies on radial orbits near pericenter can indeed show perpendicular tails. This can happen not only as a projection effect, but because at one point in a radial orbit, a galaxy would be moving perpendicular to the BCG for a short time, and would be in the process of changing tail direction. Therefore, these special cases of perpendicular tails would be an intermediate type between a tail pointing away and towards the cluster center. Although we suspect the overall perpendicular population to be dominated by circular orbits.

The right panel of Figure 3.7 further shows that tails pointing towards and perpendicular tails have a similar velocity dispersion far from the center, but tails pointing towards have the second highest dispersion at half a virial radius. This could be an indication that they are backsplashing. However, near the cluster center they have the lowest dispersion, but only after removing the unwinding galaxies. In fact, if these are not removed the velocity of towards tails in the cluster core increases so there is some uncertainty in this bin.

We also plot the VDP of the candidates with no tail and note that they have the highest dispersion near the cluster center. However, this result is highly influenced by a single galaxy (SC18) at the very top left of the diagram (an image of the galaxy is available in the appendix, in which we show the full display of the tail directions in Figure A.2). This is a JClass 2 candidate for which four classifiers saw a possible tail (three with a marginal classification), but could not agree on the direction. Therefore, the existence of a tail for this galaxy seems plausible but we lack enough indicators to determine a tail. We should keep in mind that all of these galaxies with no tail were identified as jellyfish candidates. Candidates classified as galaxies with no tail might in reality have a tail, but that is not easily visible in the available optical images. Additionally, these galaxies probably have a mixture of orbital shapes. Although, likely with a higher fraction of circular orbits (since they typically have a low JClass), especially farther from the center.

3.4 Radial distribution

Although phase-space diagrams already contain information regarding the radial distribution of the galaxies relative to the cluster center, these can only include galaxies with known radial velocities, lowering our sample size. Then, in order to inspect a more statistically relevant sample we present in Figure 3.9 the radial distributions including both confirmed members and those with unknown membership. We further distinguish between all candidates (left panel) and those with clear tails (right panel). We should note that if we see a clear tail, indicative of strong ram pressure stripping, then there should be a greater probability for a said galaxy to actually belong to the cluster, despite not having spectroscopical proof. The results obtained here might give us an early hint at the average radius where optical tails first become visible in clusters.

In general, we obtain consistent results with the ones from the smaller sample in the phase-space diagram. The away sample peaks at $\sim$ 0.5 R_{200}, with a mean clustercentric distance of 0.64 R_{200}, regardless of tail confidence. Perpendicular tails also peak at the same value but have a wider spread. They also show a larger mean radius at 0.8 R_{200} in the left panel, but for clear tails, they have the same mean radius as

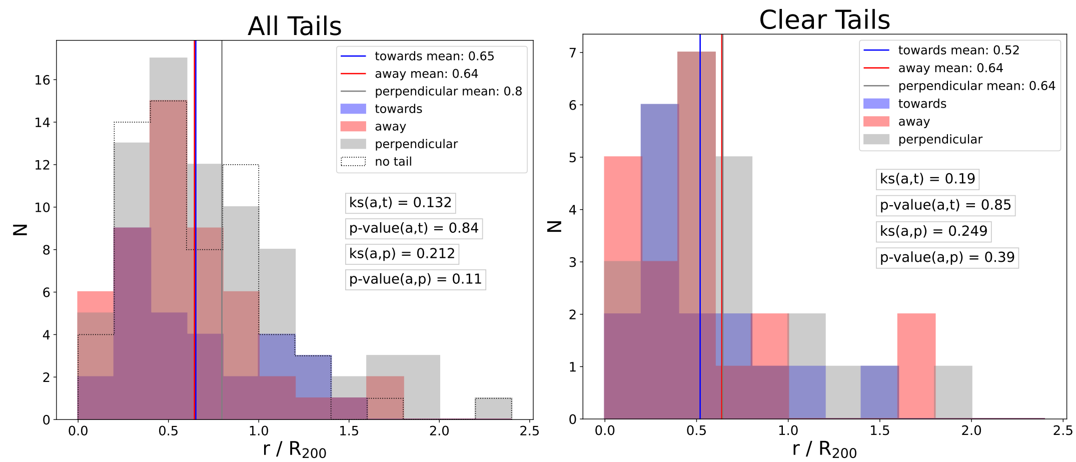

Figure 3.9: Projected radial distribution of jellyfish candidates with no tail (dotted), and tails pointing towards (blue), away (red), and perpendicular (gray) to the BCG. Left: Radial distribution for all tails. Right: Radial distribution for clear tails only. Colored solid vertical lines represent the mean of the respective distributions. All plots include the results of the Kolmorov-Smirnov test, showing the KS statistic (ks) and p-values when comparing the distributions of the tails pointing away (a) with respect to the tails pointing towards (t) and perpendicular (p) to the BCG. The distributions are excluding confirmed non-members, interacting galaxies, and interacting clusters.

the away sample. The towards sample has the same mean as the away sample in the histogram with all tails, but it is lower (0.52 R_{200}) when filtering by clear tails. Interestingly, the towards sample also presents a peak closer to the cluster center than the other orientations, further suggesting tails in outfalling galaxies do not remain visible for long after pericenter (or have changed direction). As we mentioned earlier, there is also a second peak for this subsample at a large radius, however, it becomes clearer on these plots that it is a relatively small number of galaxies, and we can see that the peak disappears when considering only clear tails. In fact, the clear tail distribution for all the sub-samples is less extended to large clustercentric distances. Lastly, the candidates with no tail show the same peak as in the away and perpendicular samples, but it is not as sharp and there is a noticeable second peak at larger distances. This could indicate that there is greater contamination of non-jellyfish galaxies in the candidates with no tail, as one would expect. Alternatively, these tails could be produced from interactions with ICM clumps, rather than the cluster itself.

We performed a Kolmogorov–Smirnov (KS) test between the away sample and the other tail orientations (results are shown in Figure 3.9), in an attempt to quantify the difference of the distributions. The resulting p-values are all larger than 0.05, suggesting the differences between the samples are not significant. In particular, the KS test between the away and towards samples surprisingly yields a very high p-value of 0.84, independently of tail clarity. On the other hand, the tests suggest the perpendicular distribution is the most different, (p-value of 0.11 when not filtering by clear tails).

The main conclusion that we can gather from these radial distributions is that jellyfish galaxies with different tail orientations follow similar distributions, being most commonly found at ~ 0.64 R_{200}. However, while galaxies in the towards sample do not show a significant difference with respect to the away sample according to the KS test, they do show a peak closer to the cluster center, suggesting optical tails might not last long after pericenter. For quantitative constraints on the lifetime of the optical tails see Section 3.6.

3.5 Dependence of tail angle on cluster and galaxy properties

S22 found that the away sample prefers higher mass hosts, lower mass galaxies, and lower mass ratios in radio continuum. Here we explore how our sample of optical jellyfish galaxies varies with cluster mass, galaxy mass, mass ratio, and galaxy color.

3.5.1 Dependance on cluster and galaxy mass

For this section, we are using the host masses (M_{200}) from Lourenco et al. (submitted) and the galaxy stellar masses from V22. On the first left three panels in Figure 3.10 we plot the distribution of the mass properties in our sample. For the first panel, we assign clusters into four different cluster subsamples, by taking the clusters hosting any galaxy within the towards, away, perpendicular, or no tail samples (note that clusters can be assigned to more than one subsample). Then, we make a M_{200} histogram for each of the cluster subsamples. From here we find that clusters hosting galaxies with perpendicular tails tend to have lower masses when compared with clusters hosting any galaxy from the away or towards samples. The clusters hosting galaxies from the towards sample appear to have about the same masses as the cluster hosting galaxies from the away sample. We apply the KS test to the away and towards samples, and we find that we cannot discard the hypothesis that they belong to the same distribution.

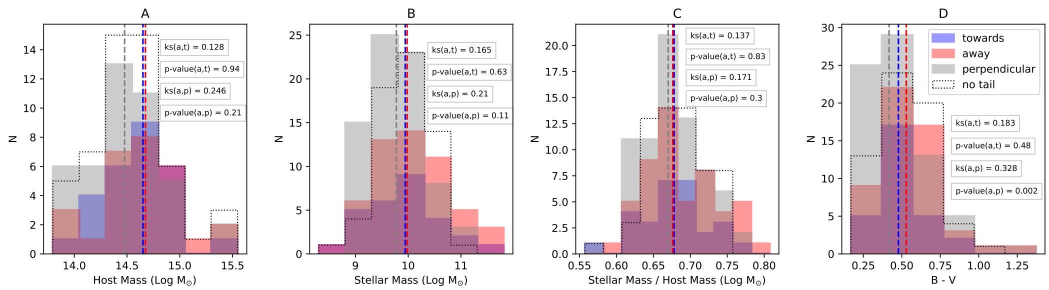

Figure 3.10: Distributions of cluster and galaxy properties for the populations of galaxies without tails (dotted), and tails pointing towards (blue), away (red), and perpendicular (gray) to the BCG. Dashed vertical lines represent the median of the samples for the blue, red, and gray histograms. All plots include the results of the Kolmorov-Smirnov test and p-values when comparing between the distributions of the tails pointing towards and away from the BCG. A: Cluster velocity dispersion distribution of clusters hosting any galaxy from a given population. B: Stellar mass velocity distributions of the galaxies. C: Stellar to host mass ratio distribution of the galaxies. D: Galaxy color distribution. All plots exclude interacting galaxies, interacting clusters, and confirmed non-members.

On the second panel in Figure 3.10 we plot the distributions of the stellar masses on each galaxy subsample, finding a similar result to the first panel, but here the difference between the perpendicular subsample and the others is slightly less noticeable. The same occurs on the third panel where we plot the distribution of the ratio between the stellar mass and the host mass.

The results in S22 show that the differences between the away and towards subsamples had more of a difference than in the results of Figure 3.10, but those results also yield low significance when applying the KS test. We should also note that in S22 the towards and away samples are defined as the angles $\theta < 90$ degrees and $\theta > 90$ degrees, respectively. Therefore, each half of the perpendicular sample was included in each of those subsamples, which could be responsible for the slightly different results.

In summary, we do not find significant mass segregation when considering different tail orientations, maybe only with the exception of perpendicular tails, which appear to prefer slightly lower mass clusters.

3.5.2 Dependance on color

We further study jellyfish tail directions as a function of color, to test (indirectly) whether the orbital history of the galaxy could be reflected in its stellar populations.

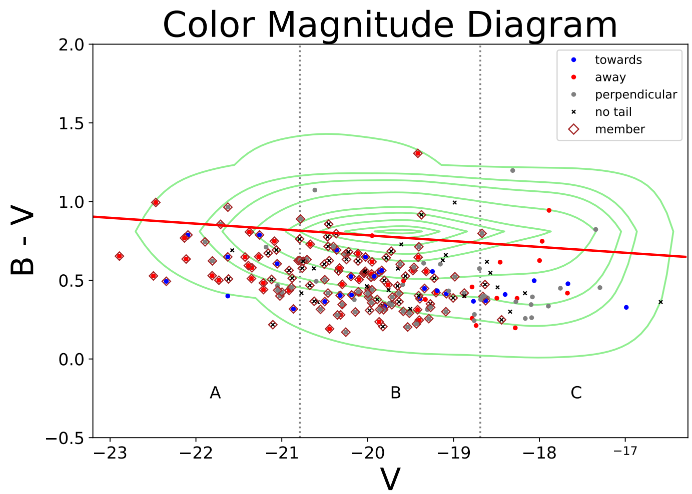

Figure 3.11: Color-Magnitude Diagram of the jellyfish candidates. The tail orientation of the galaxies is highlighted with colors; towards (blue), away (red), perpendicular (gray), and no tail (black). Confirmed members are highlighted with brown diamonds. The green contours represent the colors of all the cluster members from omegaWINGS and WINGS (including non-jellyfish candidates) and the red line represents a linear fit of the red sequence. We divided the diagram into three magnitude regions A, B, and C, going from brighter to fainter, with a width of $\sim$ 2.1 V-mag. This plot excludes interacting galaxies, interacting clusters, and confirmed non-members.

In Figure 3.10 we see a greater difference in color between the subsamples (although not very significant) than in the mass comparisons. Because of this, we inspect in more detail how the measured tail angles depend on galaxy color, which is a broad indicator of the age of the stellar populations of the galaxies. In Figure 3.11 we show the color-magnitude diagram (CMD) of the sample of jellyfish galaxies and, for reference, the sample of WINGS and omegaWINGS cluster galaxies in the background, where the red sequence of passive galaxies is clearly separated from the blue cloud of star-forming ones. Most jellyfish candidates belong to the blue cloud, as expected of gas-rich late-type galaxies that have not yet been completely stripped.

From the last panel of Figure 3.10 we find that perpendicular tails have the bluest colors, which is consistent with quenching having the greater impact for galaxies on radial orbits bringing them closer to the core, which is expected of the towards and away samples. Furthermore, this is the only case where the KS test yields a low p-value (0.002), confirming that the colors of perpendicular tails follow a significantly different distribution from the other tail orientations. Interestingly, the jellyfish galax-

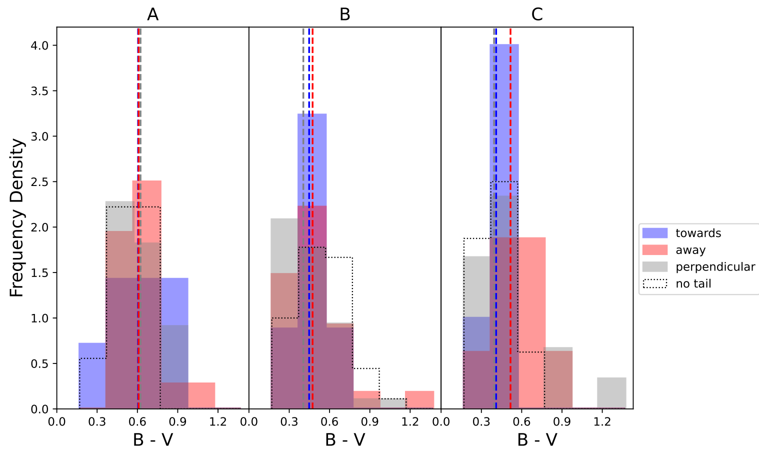

Figure 3.12: Normalized color distribution of jellyfish candidates with no tail (dotted), and tails pointing towards (blue), away (red), and perpendicular (gray) to the BCG, within the three magnitude regions (A, B, and C) from Figure 3.11, going from brighter (left) to fainter (right). Dashed vertical lines represent the median of the samples for the blue, red, and gray histograms. From here we note that the slightly bluer distribution obtained in the last panel of Figure 3.10 for the galaxies pointing towards is mostly caused by the fainter end of the distribution.

ies with tails pointing towards the cluster center (presumably post-pericentric passage) also have slightly bluer colors than the ones pointing away from the cluster (infalling). This is surprising because we expect outfalling galaxies to potentially have experienced more quenching since ram pressure would have been acting for a longer time. One possibility is that star formation is temporarily enhanced at the peak of the stripping process, as seen in Jaffé et al. (e.g. 2016). However, it should be noted that the color difference we find is not significant, according to a KS test. If we go back to Figure 3.11 and split the CDM into three regions from brightest to faintest (left to right; A, B, C, respectively), we can re-inspect the color distribution in each of these bins in Figure 3.12. From here we find that the galaxies from the towards sample in the faint end are the ones shifted to bluer colors. When inspecting these galaxies we note that four have low JClass and tail confidence. Only one galaxy has a clear tail and is the reddest of the five. Furthermore, most faint galaxies are non-confirmed members. Therefore, the slight difference in color between the away and towards samples is only caused by a small number of low-confidence measurements.

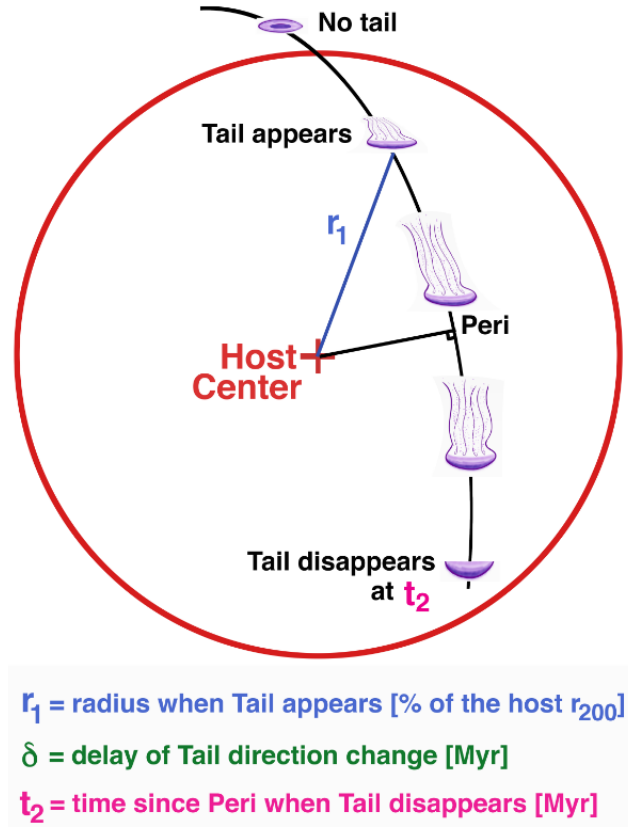

Figure 3.13: Schematic from S22 illustrating the key parameters of the model.

3.6 Lifetime of optical tails in stripped galaxies

In order to use our tail direction results to help constrain the lifetime of optical tails of jellyfish galaxies in clusters, we compare our results with models generated from simulation data following the method introduced by S22. In short, this method uses N-body cosmological dark matter only simulations, in which the galaxy tails are later added using an MCMC model with three free parameters; r_1, δ, t_2 (see Figure 3.13). The parameter r_1 is the 3D distance from the cluster center at which the tails first become visible. The tail direction is expected to be opposite to the direction of motion of the galaxy. However, if the galaxy changes orbital direction, it takes some time for the tail to change direction (see Roediger & Brüggen 2007, Tonnesen 2019). To account for this the parameter δ is used to set the delay that takes for the tail to change direction when the galaxy has changed its orbital direction. Lastly, the parameter t_2 is the time after pericenter that it takes for the galaxies to lose their tail. If the galaxies lose their tails before pericenter, then t_2 can take negative values.

S22 used radio continuum tail observations from Roberts et al. (2021a) to constrain the three parameters using the phase-space and tail orientation distributions. They had a large sample of galaxies covering up to R_{180} (~ 1.05 R_{200}) of the cluster. Ideally, we would want a cluster sample reaching much farther than one virial radii, covering up to the infall regions. For this work, however, we have a mix of cluster coverages (ranging from 0.35 R_{200} to 2.11 R_{200}) and if we only consider clusters covered to at least a given radius (e.g. 0.7 R_{200} to maximize galaxy numbers) and we remove objects without spectroscopy (for plotting on phase-space diagram), we are left with a low number of galaxies. Therefore, we instead modify the method using the radial distribution of the galaxies together with the tail direction distribution of all galaxies in the clean sample. Note that this new method does not use phase-space so we do not have to use the spectroscopic sample. Furthermore, in the model, we mimic the conditions of our sample, by using r_{min} values (see section 3.2.2) similar to the ones we have in the observations.

To test the new model and modified method in Figure 3.14 we show a mock test of the modified model, using input values of (r_1, δ, t_2) = (76, 300, 500). From here we find that the model can easily reproduce the initial input values within the 68% credible interval, obtaining good constraints on r_1 and t_2. The success of the modified method to retrieve the r_1 and t_2 parameters provides confidence for funning the model on our data and motivates the use of this method on large photometric samples.

We then ran the model with the observations using galaxies with both marginal and clear tails, and another using only clear tails. The results are presented in Figure 3.15. In the case of all tails (top panels), we find median values of $r_1 = 1.16^{+0.07}_{-0.06}$ R_{200} and $t_2 = 659^{+281}_{-281}$ Myr, while in the case of only clear tails (lower panels), we find $r_1 = 1.02^{+0.08}_{-0.08}$ R_{200} and $t_2 = 552^{+332}_{-234}$ Myr. Both results are in fairly good agreement within errors and indicate that the tails are formed very early upon entering the cluster, and disappear shortly after pericenter. It is also expected that clear tails seem to appear a bit further into the cluster, when ram pressure starts to overcome the anchoring force of the galaxies during the first infall into the cluster.

Overall our results indicate that ram pressure stripping is a strong and fast process affecting galaxies as they cross the intracluster medium for the first time.

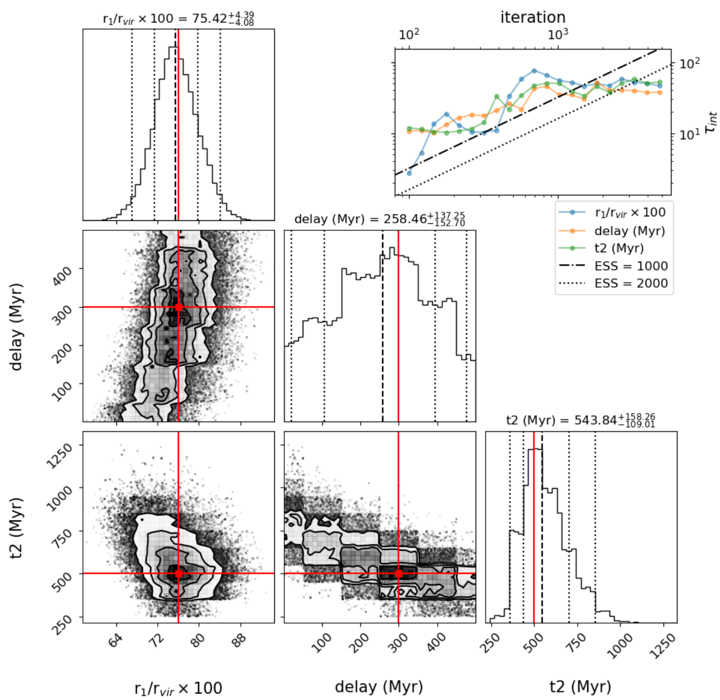

Figure 3.14: MCMC mock test (as in S22). For each case, panels are arranged as follows. In the upper right, a convergence monitoring panel is shown for each parameter. The panels with grayscale shading and contours are 2D PDFs comparing two different model parameters. The upper left, center, and lower right panels are marginalized PDFs of r_1/R_{200}, δ, and t_2, respectively. The central vertical dashed lines are the median of the respective distributions, while the surrounding vertical dashed lines show the 68% and 95% credible intervals. The subtitles of the panels provide the median values, and the errors are for the 68% credible interval. The red lines show the input value for each parameter.

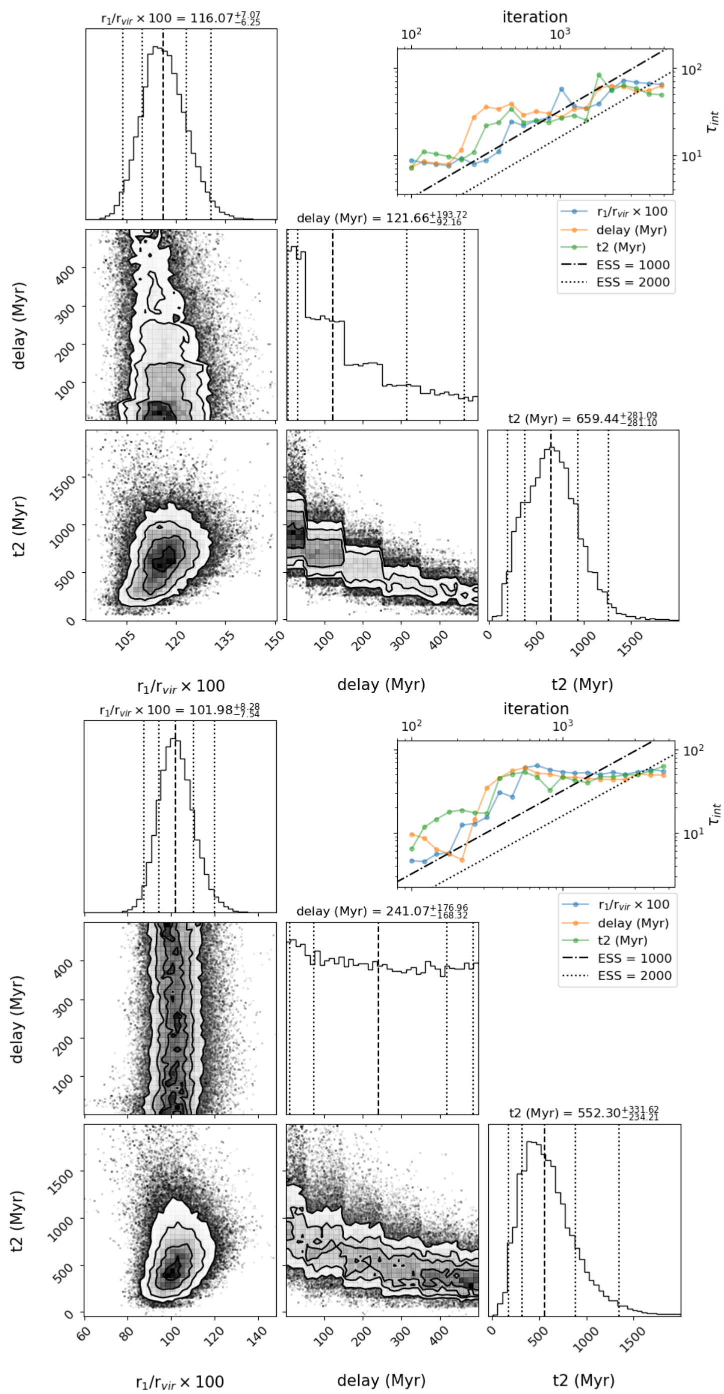

Figure 3.15: MCMC results for all tails (upper panels) and only clear confidence tails (lower panels). Panels are arranged as in Figure 3.14. Interacting galaxies, interacting clusters, and confirmed non-members are excluded from the model.

Chapter 4

Summary and Conclusions

In this work we measured and studied the projected optical tails of the largest jellyfish candidate sample in local clusters known to date (379 candidates in total, 227 when removing galaxies with signs of gravitational interactions or confirmed non-membership), taken from the works of P16 and V22 using observations from the WINGS and omegaWINGS surveys. We had up to seven classifiers to visually inspect the images of the galaxies to determine the tail directions and confidence of the tails, from which we then took an average value based on the directions that agreed within a margin of 45 degrees. We obtain good agreement between the classifiers, being able to find a tail angle for 71% of the ram pressure stripping candidate sample. We further test the accuracy of our results by comparing with tail directions measured in Hα emission by an independent classifier, finding an agreement of $\sim$ 70% within 45 degrees and an overall discrepancy with a circular average of -4.2 ± 55.9 degrees, adding support to broad-band optical tail studies.

We constructed histograms of the tail directions with respect to the cluster center using bins of 45 degrees, dividing the sample in galaxies pointing towards ($\theta < 45$ degrees), away ($\theta \geq 135$ degrees), and perpendicular (45 degrees $\leq \theta < 135$ degrees) to the direction of the BCG. From the tail distributions we find two types of possible distributions depending if we consider all jellyfish candidates with any signature characteristic of ram pressure stripping, or if we use only the more clear and extreme examples of stripping. In the former, we find that galaxies with tails pointing away from the cluster (large angles) have the highest peak, and then monotonically decrease towards smaller angles, such that 32.7% of the galaxy tails point away, 18.5% point towards, and 48.8% point perpendicular to the BCG. When using candidates with clear tails, high JClass, or clustercentric distances below $0.7R_{200}$, we find a second peak for the galaxies with tails pointing towards the BCG (small angles). Both results are consistent with ram pressure stripping being more effective for galaxies on radial orbits, especially infalling ones. Finding a noticeable fraction of tails pointing towards, albeit smaller than the other orientations, indicates the tails disappear near pericenter (or changed orbital direction), likely shortly after pericenter.

Using the JClass number defined in P16, we obtain that the strongest stripping signatures are present in galaxies pointing away, having the most cases of JClass 5 galaxies and 38% of cases with JClass > 2. Tails pointing towards also show high stripping signatures with 40% of galaxies with JClass > 2, but preferring JClass 4 rather than JClass 5 cases. In contrast, perpendicular tails only have 20% of galaxies with JClass > 2, and 5% of examples with JClass 4 or JClass 5. These results could indicate galaxies on radial orbits are more affected by ram pressure.

We compared the tail orientation subsamples in the phase-space diagram, finding that galaxies with tails pointing away have the largest velocity dispersion profile (VDP) at any clustercentric distance, while perpendicular tails have the lowest VDP (consistent with more relaxed and circular orbits). Tails pointing towards have the second largest velocity dispersion at $\sim 0.6R_{200}$, but have the lowest near the center (although with great uncertainty). We also find that galaxies with clear tails prefer high velocities near the cluster core. These results are consistent with the formalism by Gunn & Gott (1972), and confirm previous claims (by Jaffé et al. 2018) that infalling galaxies on radial orbits experience stronger ram pressure stripping.

To inspect the radial distribution of a larger sample than the available in the phase-space diagram, we also presented the radial distribution of the galaxies with confirmed membership and unknown redshift combined. We get consistent results with the ones from phase-space, finding a distribution that peaks at $\sim 0.5\ R_{200}$ for tails pointing away or perpendicular to the BCG, while tails pointing towards show a peak closer to the center, suggesting they do not last long after pericenter. We find a typical average distance that tends to be around $0.64\ R_{200}$ (depending on the tail orientation and clarity of the tails).

When comparing the properties of the galaxies (host mass, stellar mass, mass ratio, and color) we do not find significant differences between tails pointing towards and away. Perpendicular tails were the most different with respect to the other tail orientations, showing slight preferences to be hosted by less massive clusters, have lower stellar masses and mass ratios, and have bluer colors than galaxies with tails pointing away from the cluster center. But, only the color distribution of perpendicular tails yielded a significantly different distribution according to a KS test. This latter result would be consistent with quenching having a greater effect on galaxies following radial orbits.

Finally, we fed the observational results to the method introduced by S22 to obtain constraints on the lifetime of optical tails. We adapted the model to suit the coverage distribution of our sample and modified the method to use the radial distribution of jellyfish galaxies instead of the phase-space coordinates to compensate for the small spectroscopic sample. We find that optical tails appear for the first time at a cluster-centric distance of $r_1 = 1.16^{+0.07}_{-0.06}$ R_{200} and disappear $t_2 = 659^{+281}_{-281}$ Myr after pericenter, confirming ram pressure stripping is an important and fast-acting physical mechanism transforming galaxies soon after they enter a galaxy cluster for the first time. And that jellyfish tails are not visible for long after pericentric passage.

Our study, although uses the largest available sample of optical jellyfish candidates in the literature, suffers from some limitations. One of the major ones is that a small fraction of clusters in the sample covers more than 2 R_{200}. Hence, we could be missing a fraction of galaxies that produce tails very far from the cluster, since we do find some examples at these distances in the few clusters that reach that far (see also Piraino et al. submitted). How many we might be missing is unknown, and could slightly alter our constraints on the formation of the tails. More generally, the inhomogeneous coverage of clusters makes the interpretation of results more challenging, as reflected by the different tail angle distributions seen for different apertures. This essentially means that for every cluster with small coverage that we are including in the main sample, we are adding a bias against galaxies on perpendicular orbits, and possibly also against recently infalling galaxies on radial orbits.

Another limitation is the sample size (despite having the current largest sample for this work), especially after cleaning and sub-dividing the sample in different tail orientations, lowering the statistical significance of some of our results. The VDP (which is further limited by spectroscopic members) is the most affected in this regard, showing great uncertainty in the results obtained. However, with the continuously growing samples of jellyfish galaxies, we expect to find opportunities to repeat this study in the near future to further refine our results.

In summary, the aforementioned results paint a clear picture where jellyfish galaxies in clusters are generally an infalling population of galaxies on radial orbits with tails mostly pointing away from the cluster center. A significant fraction however has tangential tails, which could be due to non-radial orbits or inhomogeneities in the ICM. The results also suggest ram pressure stripping has a stronger effect on galaxies following radial orbits, while galaxies on perpendicular orbits show mild signatures of ram pressure stripping. Using the novel method introduced by S22 we find that ram pressure stripping features (tails) typically start to appear just beyond R_{200} and can be visible until shortly after pericentric passage. Remaining work will involve doing a more detailed analysis of the results of the model, such as splitting by cluster and galaxy properties, and comparing with stripped galaxies at other wavelengths. This is going to broaden our understanding of ram pressure stripping and the effect this mechanism has on the star formation of cluster galaxies.

Chapter 5

Future Perspectives

In this thesis, we have presented a methodology based on the tail classification of jellyfish galaxies, which we can use to provide quantitative constraints on the lifetime of jellyfish tails. For this purpose, we are currently working on implementing the novel method described in S22 to our sample (see Section 3.6). The objective going forwards will be to repeat this procedure in future studies with newer and larger samples to obtain better statistics and more accurate results. Likewise, we can already begin to use this procedure to obtain results in other wavelengths, with the main candidates being UV observations and Hα emission.

The method we used to measure the tail directions is one that has been continuously refined from previous studies and through this work and will continue to do so as large-scale identification and classification of jellyfish tails is becoming available with future projects. A citizen science project in the `Zooniverse.org` platform has been recently launched with the specific purpose of identifying jellyfish galaxies[1]. This project allows volunteers from around the world to help classify jellyfish candidates, including the option to draw the tail direction in a similar way as it is done in this thesis. A large number of classifiers would help obtain more accurate tail measurements. Therefore, we hope for the jellyfish Zooniverse project to perform well, as it would provide a large sample of tail measurements to work with.

[1] https://www.zooniverse.org/projects/cbellhouse/fishing-for-jellyfish-galaxies

Another area for improvement in our analysis is the sometimes subjective nature of visual classification (although we try to compensate by having a large number of classifiers). Like with the case of current morphology classification programs, automatized tail classification of jellyfish galaxies, however very difficult to do, can become a future goal to aspire to. Some attempts have been made to identify jellyfish candidates based on asymmetry parameters (e.g. Roberts et al. 2021a, Bellhouse et al. 2022), and with well-characterized visual samples like our own one and the one from the Zooniverse project we will be able to train machine learning algorithms in the near future.

Ultimately, the goal of all of these studies is to constrain the role of the environment and in particular gas stripping phenomena in galaxy evolution.

Appendix A

Appendix: Tail Measurements

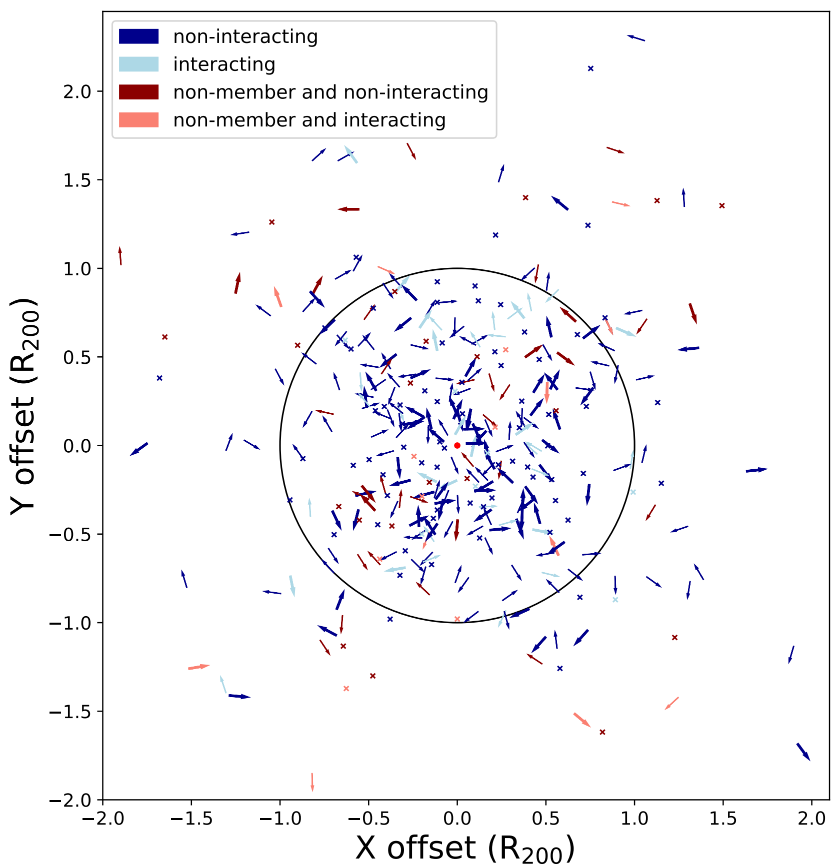

Figure A.1: Positions and tail directions of the entire parent sample (except for galaxies where R_{200} of the respective cluster is not available). The positions are plotted relative to the BCG (red dot) in the respective cluster. Arrows are pointing in the direction of the tail, and crosses indicate no tail. The confidence of the tails is represented by the width of the arrows, where clear tails are wider and marginal tails are narrower.

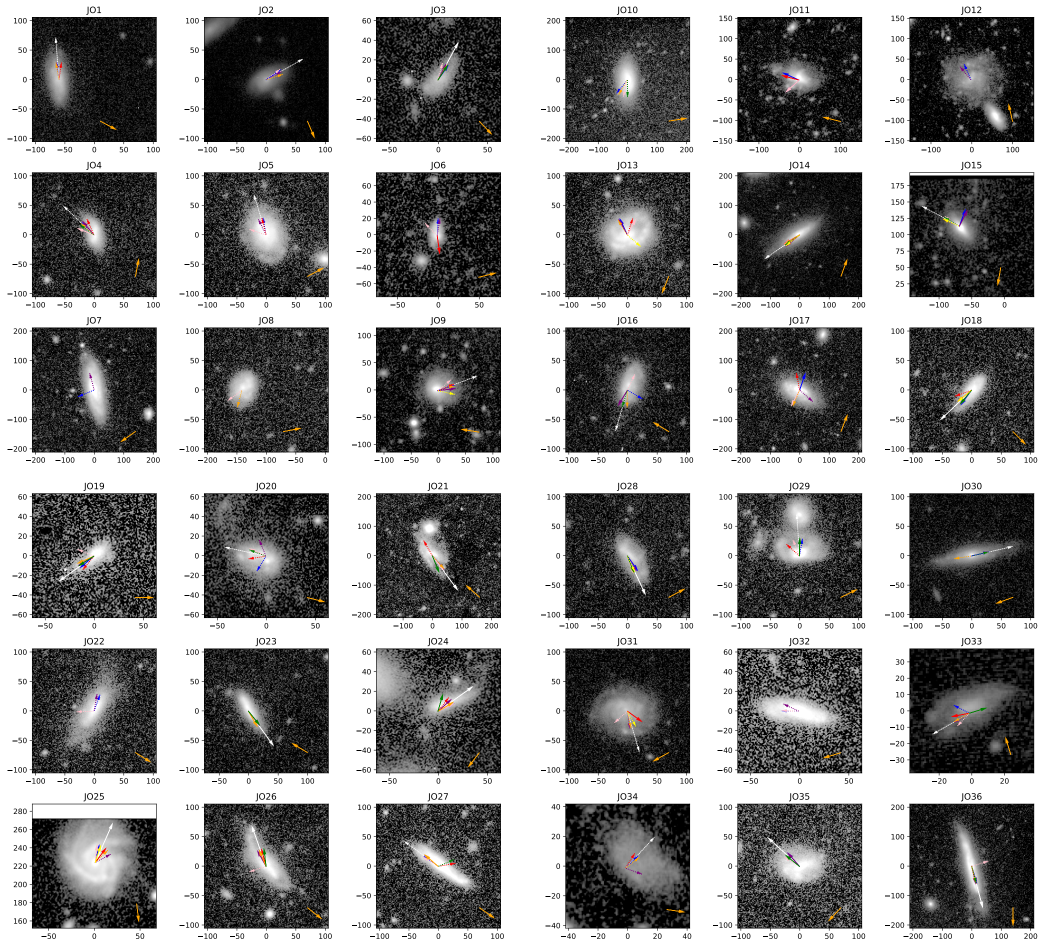

Figure A.2: B-band images from all WINGS/omegaWINGS jellyfish candidates with arrows representing the tail directions. Colored arrows are defined as in Figure 2.5.

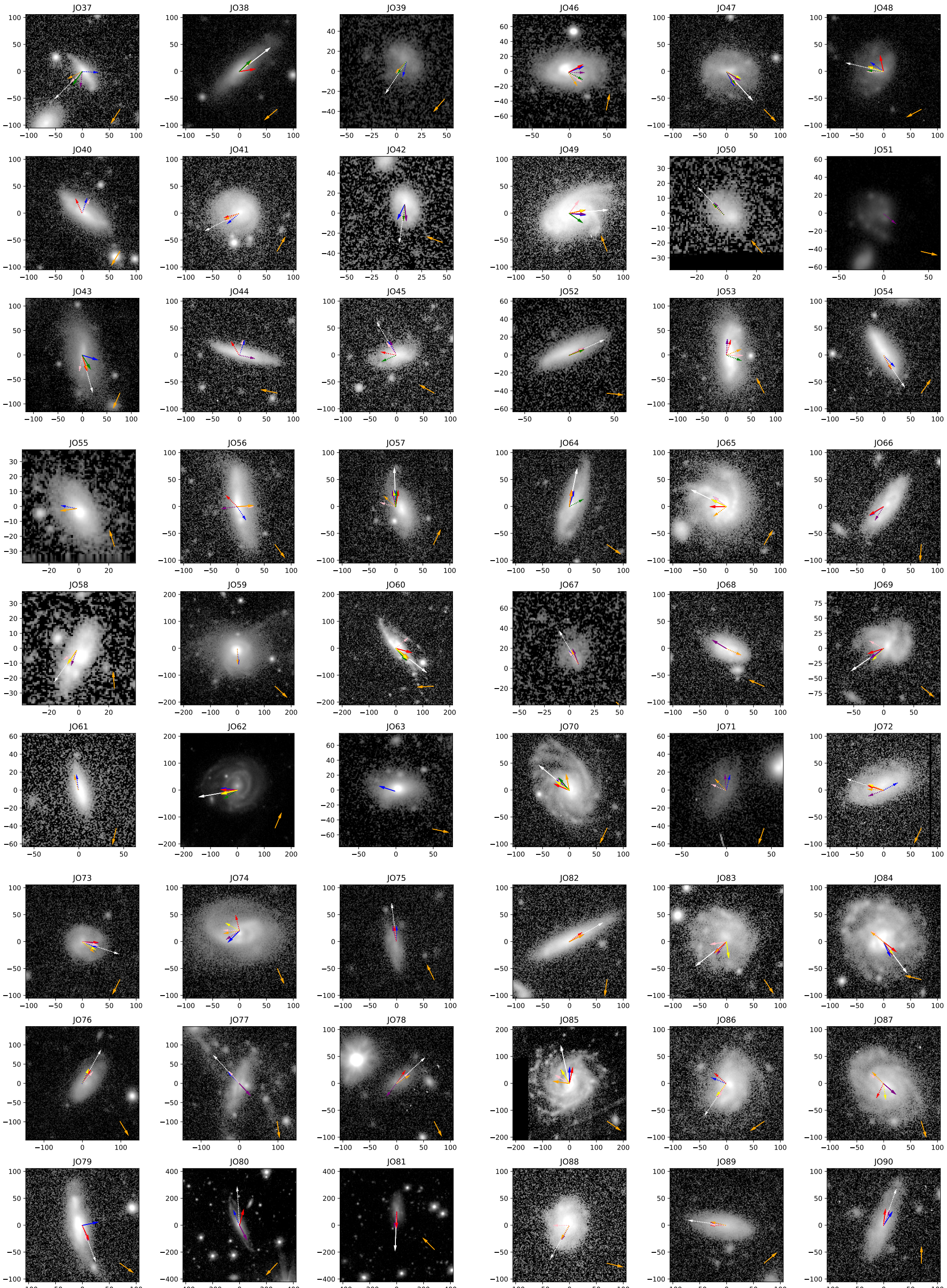

Figure A.2: Continued

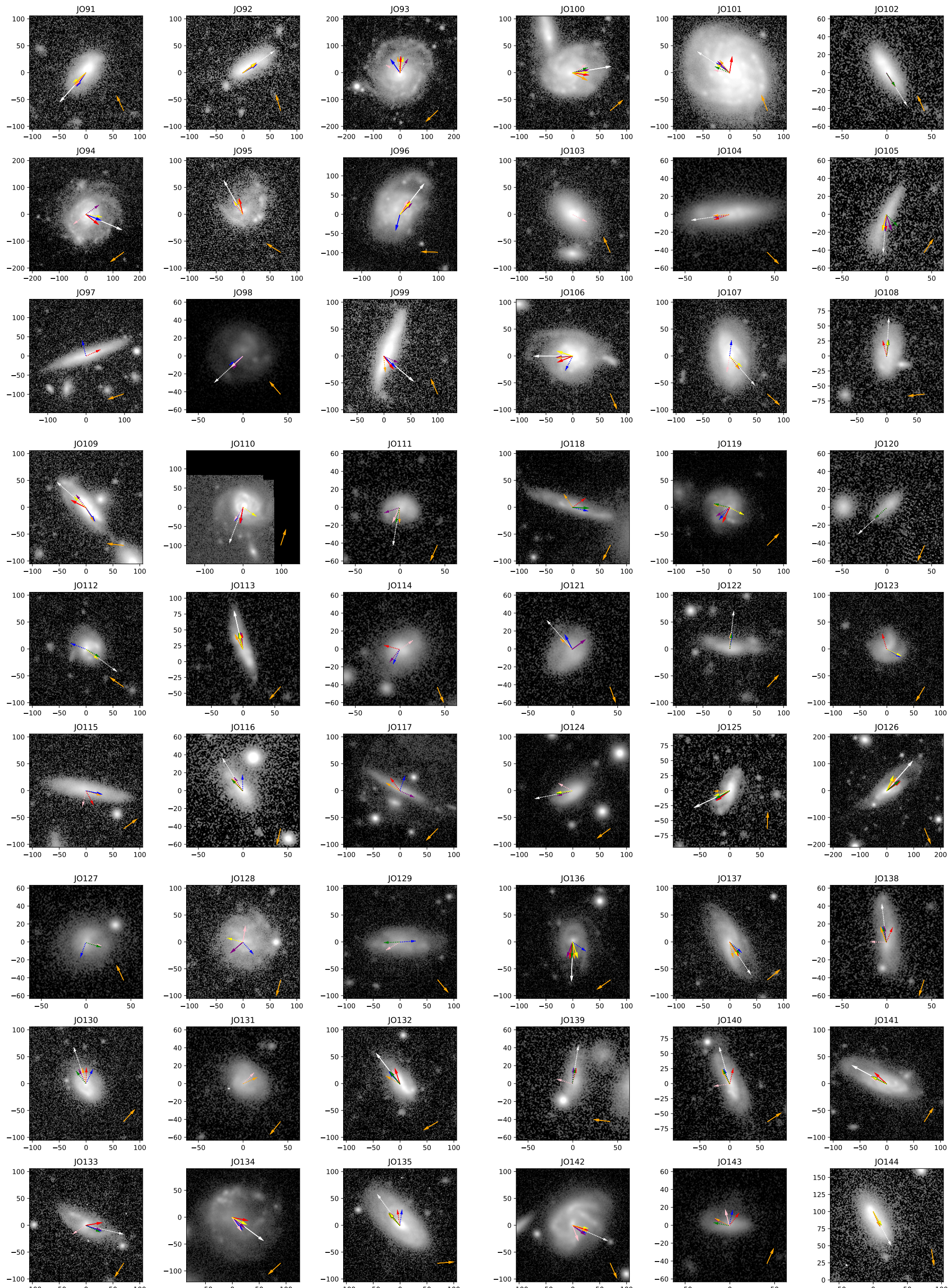

Figure A.2: Continued

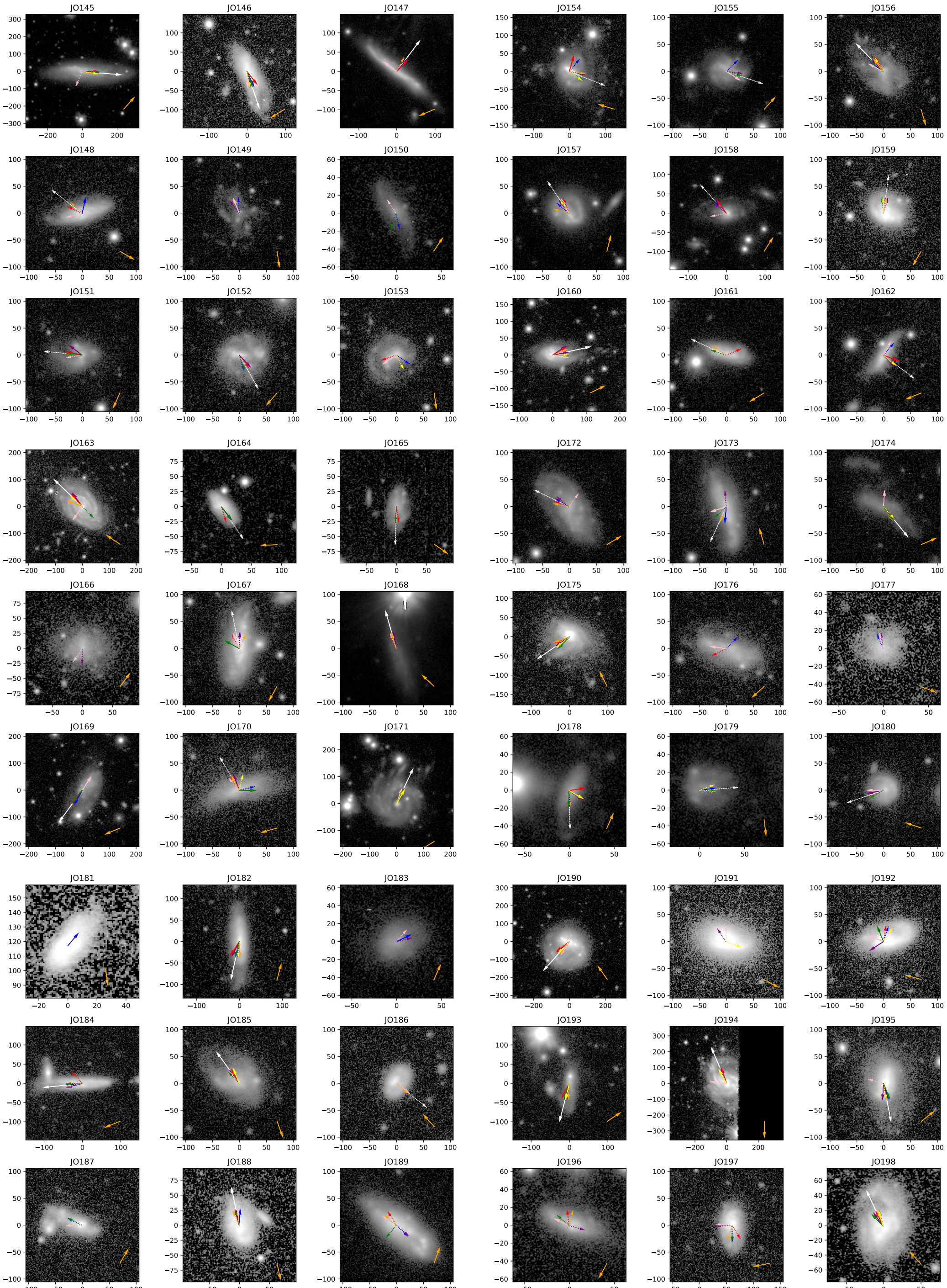

Figure A.2: Continued

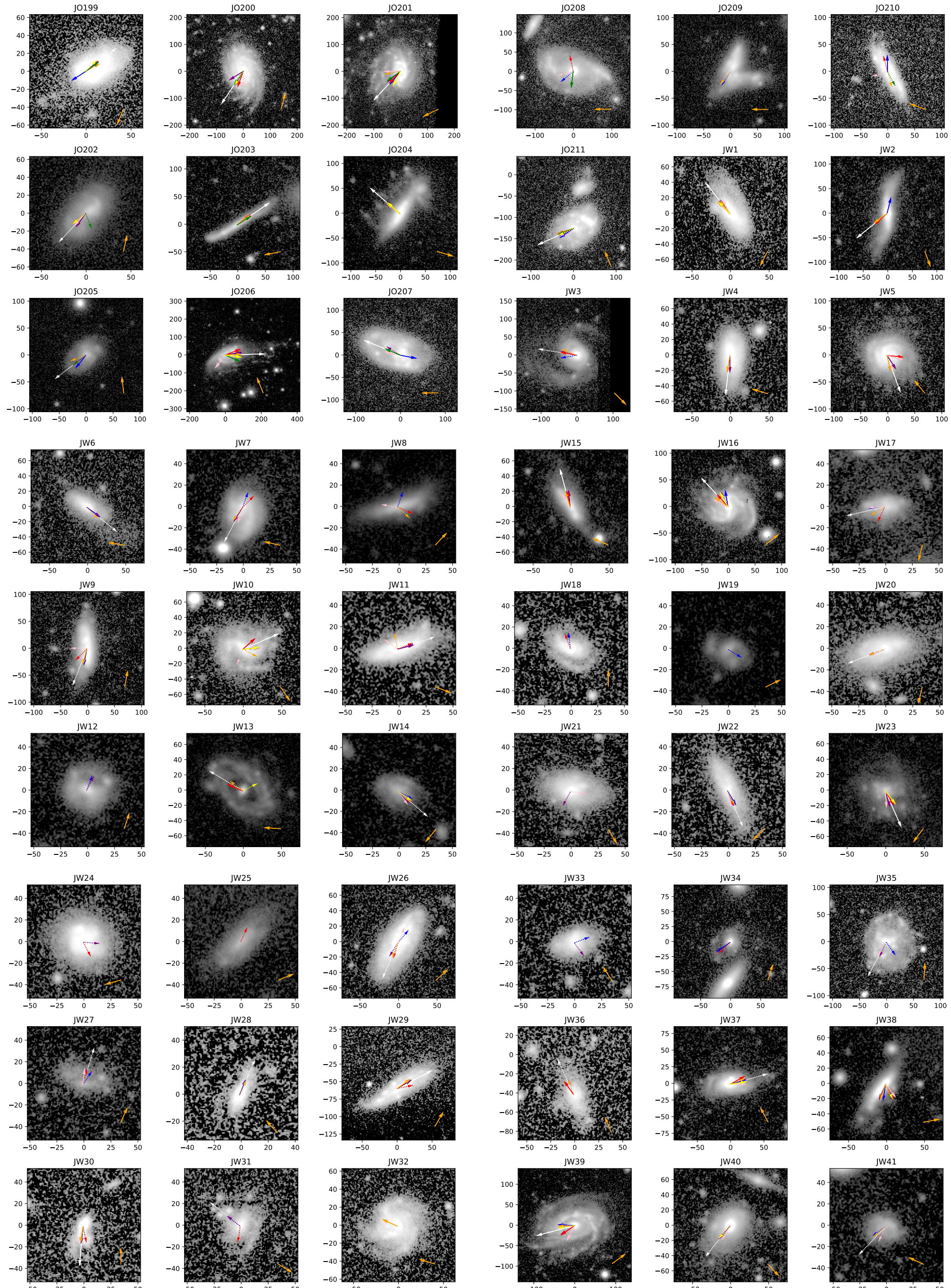

Figure A.2: Continued

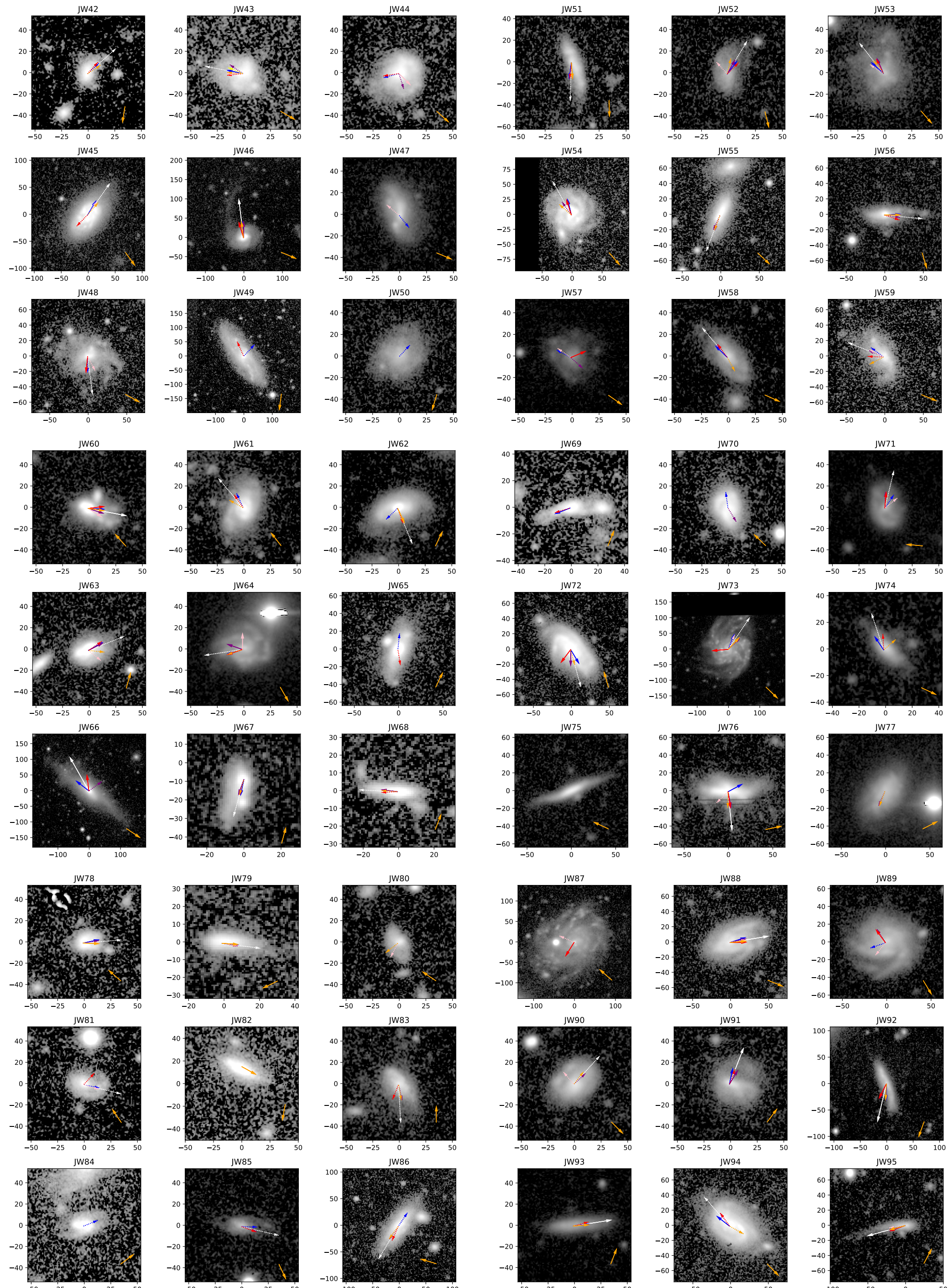

Figure A.2: Continued

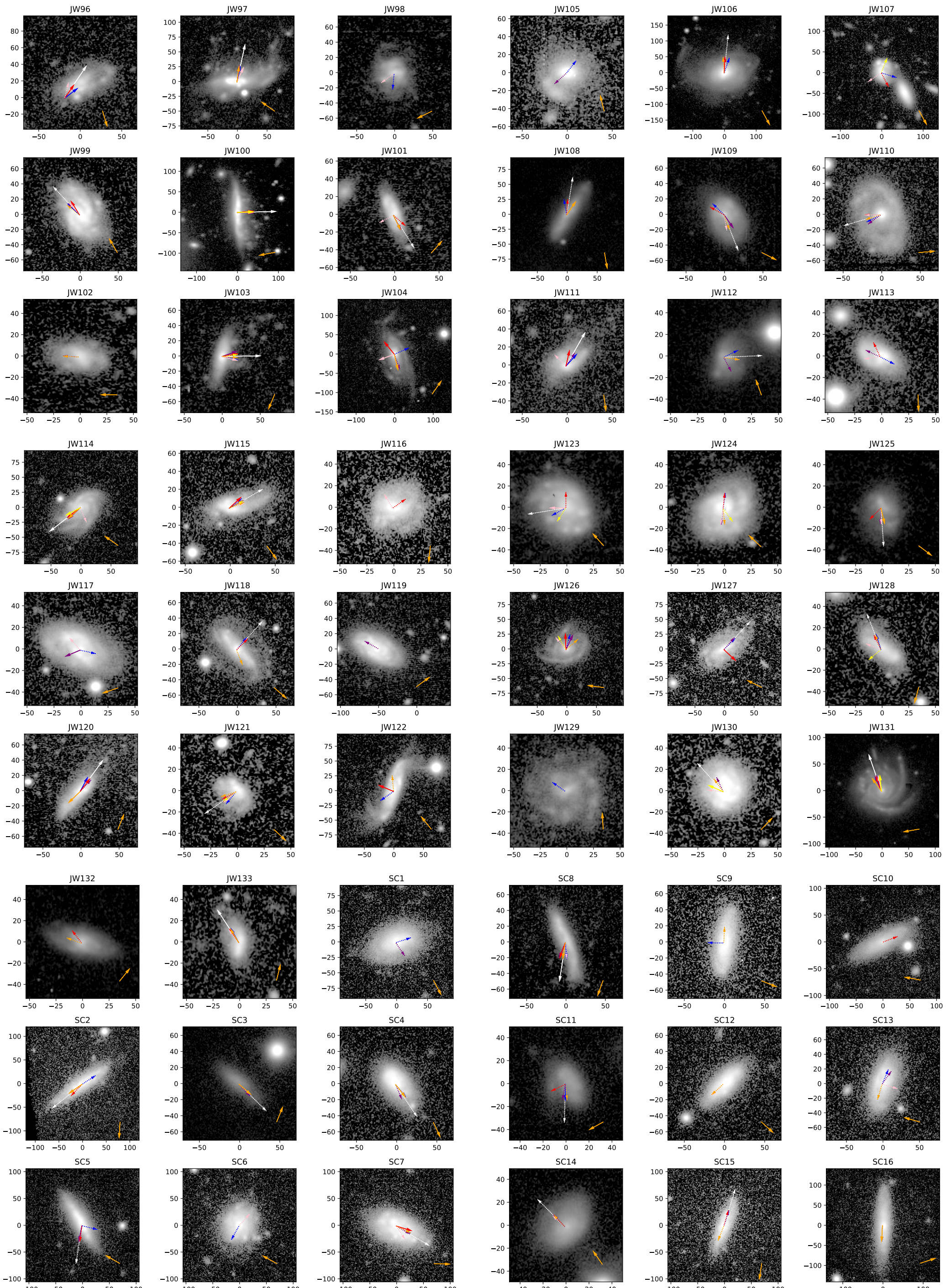

Figure A.2: Continued

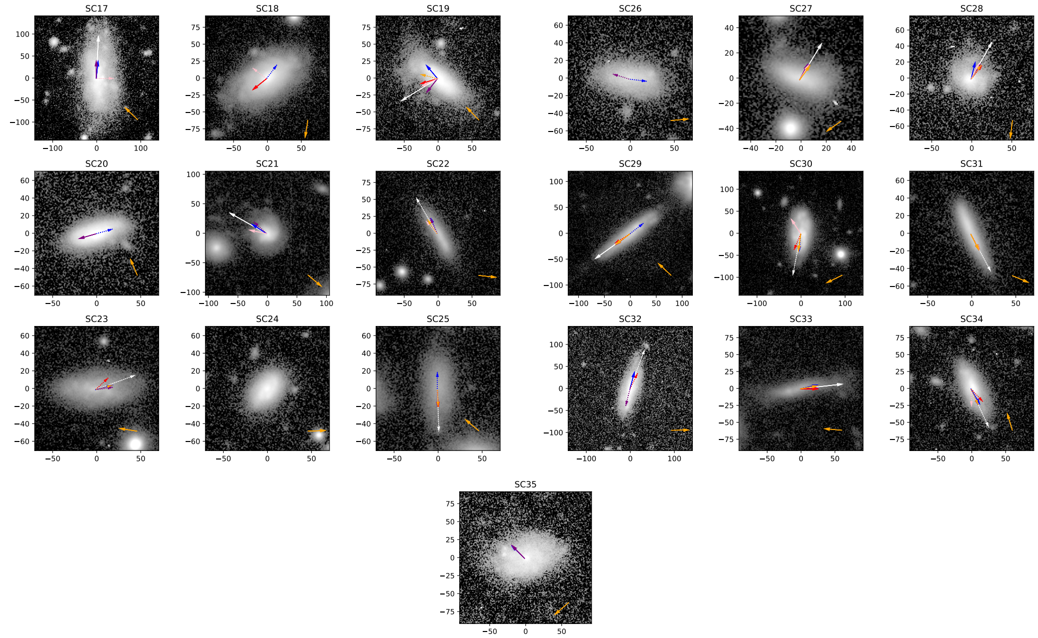

Figure A.2: Continued

Table A.1: Table of mean angles for each jellyfish candidate. The x-axis angle denotes the tail angle with respect to the x-axis (with the north pointing up and west to the right). The tail-BCG angle denotes the angle of the tail with respect to the direction to the BCG. The confidence can take the values 0, 1, or 2; representing no tail, marginal tail, or clear tail, respectively.

Galaxy	Cluster	RA (deg)	DEC (deg)	x-axis angle (deg)	Tail-BCG angle (deg)	Confidence
JO1	A1069	160.433	-8.42	94.5	122.5	1
JO2	A1069	160.109	-8.266	29.5	96.5	1
JO3	A1069	160.147	-8.463	61.6	107.6	2
JO4	A1069	159.973	-8.907	136.5	57.5	1
JO5	A1069	160.335	-8.896	106.7	78.7	1
JO6	A119	14.242	-1.299	-	-	0
JO7	A119	13.807	-1.076	-	-	0
JO8	A119	14.487	-1.336	-	-	0
JO9	A119	13.909	-1.28	20.4	150.6	1
JO10	A119	14.423	-1.312	-	-	0

Table A.1 continued from previous page

JO11	A119	13.945	-1.286	-	-	0
JO12	A119	14.015	-1.488	-	-	0
JO13	A119	13.915	-0.877	-	-	0
JO14	A147	17.094	2.073	-145.6	144.4	1
JO15	A147	17.024	2.339	151.8	108.2	1
JO16	A147	16.565	1.904	-106.3	104.7	1
JO17	A147	17.147	1.944	-	-	0
JO18	A147	17.228	2.374	-136.3	91.3	2
JO19	A147	17.498	2.196	-144.2	144.2	2
JO20	A147	17.229	2.239	167.5	178.5	1
JO21	A147	16.559	1.763	-53.6	167.4	2
JO22	A151	17.631	-15.153	-	-	0
JO23	A151	17.034	-15.512	-54.0	157.0	2
JO24	A151	17.033	-15.182	35.4	163.4	2
JO25	A151	17.222	-15.337	66.1	149.1	2
JO26	A151	17.674	-15.054	109.4	147.4	2
JO27	A151	17.702	-15.079	143.2	178.2	1
JO28	A151	17.539	-15.573	-65.0	93.0	2
JO29	A151	17.597	-15.585	93.6	67.6	1
JO30	A160	17.7	15.685	13.0	173.0	1
JO31	A160	17.841	15.708	-73.7	77.3	1
JO32	A160	17.853	15.607	-	-	0
JO33	A160	18.171	15.253	-150.2	102.8	1
JO34	A160	18.434	15.516	47.0	55.0	1
JO35	A160	17.888	15.859	137.7	89.3	2
JO36	A160	18.248	15.592	-75.0	15.0	2
JO37	A1631a	193.076	-15.162	-135.2	12.2	1
JO38	A1631a	193.013	-15.277	37.7	177.7	2
JO39	A1631a	193.197	-15.39	-123.3	7.7	1
JO40	A1631a	193.16	-15.263	-	-	0
JO41	A1631a	193.478	-15.789	-153.0	147.0	1
JO42	A1631a	193.218	-15.572	-98.0	102.0	1
JO43	A1631a	193.247	-15.364	-74.3	39.7	1
JO44	A168	18.524	0.383	-	-	0

Table A.1 continued from previous page

JO45	A168	18.319	0.202	120.7	30.3	1
JO46	A168	18.784	0.227	-	-	0
JO47	A168	18.991	0.693	-47.8	1.8	2
JO48	A168	18.481	0.567	166.9	41.1	1
JO49	A168	18.683	0.286	5.2	105.8	2
JO50	A193	21.202	8.609	133.4	2.4	1
JO51	A1983	223.752	16.816	-	-	0
JO52	A1983	223.38	16.717	24.0	30.0	1
JO53	A1983	222.976	16.222	-	-	0
JO54	A1991	223.897	18.284	-56.5	111.5	1
JO55	A1991	223.612	18.582	-	-	0
JO56	A1991	223.722	18.757	-	-	0
JO57	A1991	223.706	18.495	92.0	28.0	2
JO58	A1991	223.61	18.399	-125.5	139.5	1
JO59	A1991	223.849	18.836	-	-	0
JO60	A1991	223.465	18.651	-38.1	138.9	2
JO61	A2107	234.865	21.977	-	-	0
JO62	A2107	235.037	21.515	-170.0	123.0	2
JO63	A2107	234.953	21.791	-	-	0
JO64	A2107	235.435	22.119	78.3	113.3	2
JO65	A2107	234.963	21.704	154.3	95.3	2
JO66	A2382	327.971	-15.567	-	-	0
JO67	A2382	328.004	-15.683	120.0	167.0	1
JO68	A2399	329.092	-7.908	-	-	0
JO69	A2399	329.33	-7.779	-145.5	105.5	2
JO70	A2399	329.017	-7.327	140.5	104.5	2
JO71	A2415	331.136	-5.115	-	-	0
JO72	A2415	331.046	-5.068	162.7	82.3	1
JO73	A2415	331.108	-5.246	-18.5	98.5	1
JO74	A2415	331.392	-5.669	-	-	0
JO75	A2415	331.192	-6.079	97.0	19.0	1
JO76	A2415	331.532	-5.451	60.8	119.8	1
JO77	A2415	331.385	-5.549	132.5	145.5	1
JO78	A2457	339.181	1.999	42.2	105.2	1

Table A.1 continued from previous page

JO79	A2457	339.028	1.559	-69.3	34.3	1
JO80	A2457	338.511	1.916	93.5	133.5	1
JO81	A2589	350.638	16.441	-92.3	132.7	2
JO82	A2589	350.91	17.304	29.6	127.6	1
JO83	A2589	351.323	17.247	-141.8	85.8	2
JO84	A2589	350.541	16.673	-53.0	141.0	2
JO85	A2589	351.131	16.868	102.8	136.8	2
JO86	A2593	350.634	14.937	-124.3	21.7	1
JO87	A2593	351.158	14.886	-	-	0
JO88	A2593	351.429	14.725	-119.5	106.5	1
JO89	A2593	351.502	14.307	172.2	132.2	1
JO90	A2593	351.088	14.333	70.5	18.5	1
JO91	A2593	350.875	14.206	-131.8	113.2	2
JO92	A2593	350.976	14.292	34.8	71.2	1
JO93	A2593	350.799	14.902	-	-	0
JO94	A2657	355.683	9.596	-23.3	120.7	2
JO95	A2657	356.111	9.115	119.2	28.8	2
JO96	A2665	357.24	6.133	51.7	126.3	2
JO97	A2734	2.634	-28.791	-	-	0
JO98	A2734	2.38	-29.315	-137.3	91.7	1
JO99	A2734	2.595	-29.345	-40.0	154.0	2
JO100	A2734	3.399	-29.262	9.6	30.4	2
JO101	A2734	2.664	-29.253	146.6	35.6	1
JO102	A3128	52.27	-52.835	-57.7	171.7	1
JO103	A3128	52.397	-52.666	-	-	0
JO104	A3128	53.189	-52.127	-171.4	126.4	1
JO105	A3128	52.863	-52.942	-94.9	150.9	1
JO106	A3128	52.807	-52.078	180.0	113.0	2
JO107	A3128	52.88	-52.346	-49.0	7.0	1
JO108	A3158	55.642	-53.676	86.7	100.3	1
JO109	A3158	55.518	-53.714	138.5	35.5	1
JO110	A3158	55.999	-53.922	-111.0	177.0	1
JO111	A3158	55.512	-53.215	-99.7	14.3	1
JO112	A3158	55.025	-54.041	-35.7	179.3	1

Table A.1 continued from previous page

JO113	A3158	55.455	-53.403	102.8	126.2	2
JO114	A3266	68.219	-60.966	-	-	0
JO115	A3266	68.269	-61.612	-	-	0
JO116	A3395	96.732	-54.021	121.9	135.1	1
JO117	A3395	96.291	-54.077	-	-	0
JO118	A3395	96.54	-54.034	-	-	0
JO119	A3395	97.496	-54.794	-	-	0
JO120	A3528	193.425	-28.734	-137.5	23.5	1
JO121	A3528	193.849	-28.786	131.4	158.6	1
JO122	A3528	193.856	-29.401	84.0	37.0	1
JO123	A3528	193.254	-28.615	-	-	0
JO124	A3528	193.083	-28.852	-168.3	24.3	1
JO125	A3528	193.675	-29.326	-154.7	117.3	2
JO126	A3528	193.865	-28.797	48.9	116.9	2
JO127	A3530	193.655	-30.808	-	-	0
JO128	A3530	193.737	-29.836	-	-	0
JO129	A3530	194.342	-29.887	-	-	0
JO130	A3530	194.453	-30.858	108.4	61.4	1
JO131	A3530	193.423	-29.843	-	-	0
JO132	A3530	193.662	-30.231	127.8	82.2	2
JO133	A3530	193.529	-29.846	-13.1	109.9	1
JO134	A3530	193.659	-30.157	-36.5	101.5	2
JO135	A3530	194.268	-30.375	125.8	120.8	1
JO136	A3532	194.106	-30.223	-91.7	53.3	2
JO137	A3532	194.679	-30.597	-56.8	95.8	1
JO138	A3532	194.244	-30.102	96.6	155.4	1
JO139	A3532	193.888	-30.415	80.8	92.2	1
JO140	A3532	194.53	-30.47	105.8	72.8	1
JO141	A3532	194.66	-30.792	151.9	94.9	2
JO142	A3556	201.198	-31.342	-23.6	42.4	1
JO143	A3556	201.267	-32.116	-	-	0
JO144	A3556	201.135	-31.116	-62.2	18.8	1
JO145	A3556	201.518	-32.129	-5.0	53.0	2
JO146	A3556	200.527	-31.412	-71.3	77.7	2

Table A.1 continued from previous page

JO147	A3558	201.707	-31.396	53.0	150.0	2
JO148	A3558	202.522	-31.231	142.3	172.3	1
JO149	A3558	202.044	-31.164	-	-	0
JO150	A3558	202.281	-31.863	-	-	0
JO151	A3558	201.805	-31.144	174.2	71.8	1
JO152	A3558	201.662	-31.171	-60.5	70.5	1
JO153	A3558	202.063	-31.033	-	-	0
JO154	A3558	201.702	-31.572	-21.8	175.2	1
JO155	A3558	202.164	-31.661	-18.6	66.6	1
JO156	A3558	202.144	-31.024	134.3	151.7	2
JO157	A3558	202.076	-31.805	124.0	48.0	1
JO158	A3558	202.28	-31.88	132.3	75.3	1
JO159	A3558	201.649	-30.993	82.0	158.0	1
JO160	A3558	202.369	-31.657	12.4	13.6	2
JO161	A3560	202.561	-32.859	155.3	55.7	1
JO162	A3560	202.874	-33.055	-37.0	121.0	1
JO163	A3560	202.916	-33.243	136.3	9.7	2
JO164	A3560	202.874	-33.128	-55.8	122.2	1
JO165	A3560	203.208	-33.078	-92.0	57.0	1
JO166	A3560	203.205	-33.243	-	-	0
JO167	A3560	202.85	-32.743	101.2	139.8	1
JO168	A3560	202.82	-33.361	106.0	31.0	2
JO169	A3560	202.636	-32.97	-126.3	30.7	2
JO170	A3667	302.713	-56.766	120.5	75.5	1
JO171	A3667	302.561	-56.642	64.6	146.4	2
JO172	A3716	313.424	-52.79	154.2	123.2	1
JO173	A3716	312.749	-53.124	-114.6	139.4	1
JO174	A3716	313.454	-52.752	-51.0	74.0	2
JO175	A3716	312.823	-52.823	-145.4	97.6	2
JO176	A3809	326.249	-43.574	-	-	0
JO177	A3809	327.295	-43.752	-	-	0
JO178	A3809	327.019	-44.344	-88.3	154.3	1
JO179	A3809	326.78	-43.705	4.8	87.8	1
JO180	A3809	326.313	-44.009	-161.1	37.9	1

Table A.1 continued from previous page

JO181	A3880	337.016	-30.301	-	-	0
JO182	A3880	337.005	-30.667	-102.5	177.5	2
JO183	A3880	337.088	-30.793	-	-	0
JO184	A3880	336.509	-30.412	-174.2	16.2	2
JO185	A3880	337.173	-30.1	125.7	164.3	2
JO186	A3880	336.76	-30.783	-38.2	170.2	1
JO187	A3880	337.199	-30.912	-	-	0
JO188	A3880	337.016	-30.415	101.7	179.7	2
JO189	A3880	337.141	-30.962	-	-	0
JO190	A3880	336.724	-30.886	-132.0	103.0	2
JO191	A4059	359.483	-34.658	-	-	0
JO192	A4059	358.697	-34.88	-	-	0
JO193	A4059	359.566	-34.928	-104.4	137.4	2
JO194	A4059	359.253	-34.681	113.0	157.0	2
JO195	A754	137.551	-9.952	-78.8	116.8	2
JO196	A754	137.026	-9.433	-	-	0
JO197	A754	136.636	-9.524	-	-	0
JO198	A754	136.883	-9.898	115.1	17.9	2
JO199	A85	10.31	-8.932	37.0	149.0	1
JO200	A85	10.521	-9.534	-123.9	161.1	2
JO201	A85	10.376	-9.263	-132.8	21.2	2
JO202	A957x	153.472	-1.195	-133.2	149.8	1
JO203	A957x	153.26	-0.897	34.5	156.5	2
JO204	A957x	153.445	-0.914	139.1	156.1	2
JO205	IIZW108	318.442	2.239	-142.8	120.2	1
JO206	IIZW108	318.448	2.477	1.6	110.4	2
JO207	MKW3s	230.74	8.04	157.7	22.3	2
JO208	MKW3s	230.308	7.372	-	-	0
JO209	MKW3s	230.41	8.144	-	-	0
JO210	Z8852	347.374	7.46	-	-	0
JO211	Z8852	347.449	7.048	-155.6	91.4	2
JW1	A133	15.55	-21.659	128.2	114.8	2
JW2	A133	15.762	-21.661	-141.0	71.0	2
JW3	A133	15.822	-21.746	170.7	144.3	1

Table A.1 continued from previous page

JW4	A133	15.427	-21.951	-96.3	100.7	2
JW5	A133	15.563	-22.011	-70.0	161.0	2
JW6	A311	32.227	19.756	-39.0	150.0	1
JW7	A311	32.001	19.698	-118.0	75.0	1
JW8	A376	41.587	36.845	-	-	0
JW9	A500	69.74	-22.209	-111.4	169.6	1
JW10	A500	69.826	-21.964	23.5	79.5	2
JW11	A500	69.941	-22.03	18.0	39.0	1
JW12	A500	69.775	-22.269	-	-	0
JW13	A602	118.143	29.347	149.0	27.0	1
JW14	A671	127.059	30.505	-40.7	89.3	1
JW15	A671	127.042	30.398	105.0	52.0	2
JW16	A671	127.364	30.276	133.0	95.0	2
JW17	A1291	173.056	56.057	-167.1	63.1	1
JW18	A1291	173.097	55.732	-	-	0
JW19	A1291	173.183	55.944	-	-	0
JW20	A1644	194.255	-17.226	-159.3	56.3	1
JW21	A1644	194.408	-17.233	-	-	0
JW22	A1644	194.204	-17.328	-66.8	71.2	1
JW23	A1644	194.245	-17.342	-66.2	60.8	2
JW24	A1644	194.089	-17.352	-	-	0
JW25	A1644	194.549	-17.504	-	-	0
JW26	A1644	194.5	-17.59	-113.7	156.7	1
JW27	A1644	194.375	-17.576	73.0	7.0	1
JW28	A1644	194.095	-17.625	66.3	65.7	1
JW29	A1644	194.456	-17.666	27.5	32.5	2
JW30	A1644	194.297	-17.651	-95.2	174.8	2
JW31	A1644	194.482	-17.306	141.5	172.5	1
JW32	A1644	194.061	-17.479	-	-	0
JW33	A1644	194.181	-17.578	-	-	0
JW34	A1644	194.366	-17.617	-	-	0
JW35	A1644	194.315	-17.655	-118.0	156.0	1
JW36	A1644	194.184	-17.663	114.3	1.3	1
JW37	A1668	195.867	19.133	15.7	102.3	1

Table A.1 continued from previous page

JW38	A1668	195.968	19.267	-	-	0
JW39	A1668	196.032	19.211	-165.4	158.6	2
JW40	A1668	196.149	19.469	-128.6	82.6	1
JW41	A1668	195.876	19.241	-133.7	71.3	1
JW42	A1668	195.924	19.385	41.7	140.7	1
JW43	A1668	196.099	19.356	169.1	160.9	1
JW44	A1668	196.14	19.439	-	-	0
JW45	A1736	202.031	-27.021	54.7	108.7	1
JW46	A1736	202.022	-27.31	97.0	120.0	2
JW47	A1736	201.99	-27.324	-	-	0
JW48	A1736	201.901	-27.333	-82.8	53.8	1
JW49	A1736	201.605	-26.959	-	-	0
JW50	A1736	201.522	-26.972	-	-	0
JW51	A1736	201.692	-27.016	-91.7	2.7	1
JW52	A1736	201.801	-27.009	59.0	135.0	1
JW53	A1736	201.995	-27.12	128.4	177.4	1
JW54	A1736	201.934	-27.184	119.2	168.2	1
JW55	A1736	201.917	-27.247	-111.0	68.0	1
JW56	A1736	201.763	-27.216	-5.5	67.5	1
JW57	A1736	201.897	-27.305	-	-	0
JW58	A1736	202.01	-27.31	130.3	154.3	1
JW59	A1736	201.931	-27.351	157.9	179.9	1
JW60	A1795	207.029	26.405	-10.8	142.8	2
JW61	A1795	207.179	26.547	130.2	2.2	1
JW62	A1795	207.233	26.566	-67.5	131.5	1
JW63	A1795	207.303	26.334	21.5	52.5	1
JW64	A1795	207.322	26.752	-171.3	111.3	1
JW65	A1795	207.348	26.359	-	-	0
JW66	A1795	207.422	26.717	119.5	153.5	2
JW67	A1795	207.298	26.322	-105.7	179.3	1
JW68	A1795	207.307	26.387	177.3	108.3	1
JW69	A1795	207.307	26.396	-	-	0
JW70	A1831	209.602	27.794	-	-	0
JW71	A1831	209.566	27.956	76.4	98.6	1

Table A.1 continued from previous page

JW72	A1831	209.75	27.78	-74.8	179.2	1
JW73	A1831	209.914	28.061	56.0	100.0	1
JW74	A1831	209.971	28.042	108.5	133.5	1
JW75	A2124	236.178	36.084	-	-	0
JW76	A2124	236.344	36.092	-84.0	96.0	2
JW77	A2124	236.441	36.028	-	-	0
JW78	A2124	236.039	35.964	4.7	134.3	1
JW79	A2124	236.05	36.186	-7.4	146.6	1
JW80	A2124	236.063	36.01	-	-	0
JW81	A2124	236.106	35.94	-13.5	137.5	1
JW82	A2149	240.292	54.189	-	-	0
JW83	A2149	240.367	53.89	-86.8	176.8	1
JW84	A2149	240.558	53.862	-	-	0
JW85	A2149	240.457	54.063	-13.4	51.6	1
JW86	A2169	243.031	49.099	-121.3	75.7	1
JW87	A2169	242.986	48.898	-	-	0
JW88	A2169	243.616	49.222	9.4	31.4	2
JW89	A2169	243.688	49.399	-	-	0
JW90	A2169	243.722	49.341	47.5	92.5	1
JW91	A2169	243.772	48.941	68.7	15.7	2
JW92	A2256	255.843	78.782	-103.2	6.8	2
JW93	A2256	256.549	78.41	9.0	60.0	2
JW94	A2256	257.291	78.875	131.0	177.0	1
JW95	A2256	256.597	78.455	-164.8	133.2	2
JW96	A2572a	349.391	18.976	56.0	129.0	2
JW97	A2622	353.724	27.352	77.8	67.2	2
JW98	A2626	354.039	21.186	-	-	0
JW99	A2626	354.077	21.067	133.0	13.0	1
JW100	A2626	354.104	21.151	1.5	170.5	2
JW101	A2626	354.358	20.91	-57.5	105.5	1
JW102	A2626	353.917	21.146	-	-	0
JW103	A2626	354.111	21.182	1.0	114.0	2
JW104	A2717	0.886	-36.033	-	-	0
JW105	A2717	0.752	-36.111	-	-	0

Table A.1 continued from previous page

JW106	A3164	56.481	-57.197	84.0	145.0	1
JW107	A3164	56.138	-57.175	-	-	0
JW108	A3376	90.2	-39.919	80.8	160.8	1
JW109	A3376	90.429	-39.944	-68.3	41.3	1
JW110	A3490	176.46	-34.442	-163.8	168.8	1
JW111	A3490	176.337	-34.414	60.3	142.3	2
JW112	A3490	176.29	-34.533	2.5	107.5	1
JW113	A3490	176.338	-34.345	-	-	0
JW114	A3490	176.182	-34.52	-142.2	72.8	2
JW115	A3497	180.2	-31.228	29.7	83.7	1
JW116	A3497	179.905	-31.241	-	-	0
JW117	A3497	179.75	-31.472	-	-	0
JW118	A3497	180.268	-31.287	48.0	89.0	1
JW119	RX0058	14.926	26.651	-	-	0
JW120	RX0058	14.652	26.738	54.0	14.0	2
JW121	RX0058	14.789	27.023	-145.2	102.2	1
JW122	RX1022	155.377	38.309	-	-	0
JW123	RX1740	264.892	35.428	-170.8	57.2	1
JW124	RX1740	264.902	35.469	-	-	0
JW125	RX1740	265.377	35.794	-86.0	49.0	1
JW126	Z1261	109.02	53.375	-	-	0
JW127	Z1261	108.583	53.216	47.0	107.0	1
JW128	Z1261	109.08	53.594	111.3	143.7	1
JW129	Z1261	109.152	53.176	-	-	0
JW130	Z2844	150.858	32.528	132.2	86.2	1
JW131	Z8338	272.424	49.947	109.1	80.9	2
JW132	Z8338	272.993	49.734	-	-	0
JW133	Z8338	272.848	49.717	123.2	47.2	2
SC1	A1069	160.082	-8.409	-	-	0
SC2	A151	17.196	-15.106	-141.3	48.3	1
SC3	A168	18.818	0.235	-44.3	112.3	1
SC4	A193	21.477	9.122	-56.3	8.7	1
SC5	A1983	222.823	16.475	-99.0	111.0	1
SC6	A2107	234.68	21.662	-	-	0

Table A.1 continued from previous page

SC7	A2107	235.415	21.794	-30.7	29.7	1
SC8	A2256	255.844	78.782	-98.6	11.4	2
SC9	A2382	328.106	-15.658	-	-	0
SC10	A2382	327.518	-15.789	-	-	0
SC11	A2382	327.834	-15.626	-91.7	59.3	1
SC12	A2382	328.283	-15.448	-	-	0
SC13	A2382	327.856	-15.74	-	-	0
SC14	A2399	329.035	-8.157	134.7	9.7	1
SC15	A2399	329.167	-7.268	73.0	172.0	1
SC16	A2415	331.638	-5.832	-	-	0
SC17	A2589	350.638	16.448	87.0	49.0	2
SC18	A2593	351.071	14.72	-	-	0
SC19	A2593	351.001	14.564	-148.4	77.6	2
SC20	A3128	52.369	-52.71	-	-	0
SC21	A3128	52.58	-52.518	150.6	169.4	2
SC22	A3556	201.299	-31.644	120.2	126.2	1
SC23	A3560	202.562	-33.208	20.1	150.9	1
SC24	A3560	203.294	-33.141	-	-	0
SC25	A3667	302.177	-57.252	-88.0	132.0	1
SC26	A3667	304.028	-56.869	-	-	0
SC27	A3667	302.661	-56.653	58.8	156.2	2
SC28	A3667	303.062	-56.6	60.6	157.6	2
SC29	A3716	312.463	-52.92	-144.3	78.7	2
SC30	A3716	312.199	-52.392	-101.0	53.0	1
SC31	A3809	327.088	-43.796	-61.8	38.8	1
SC32	A3880	337.427	-30.583	69.5	68.5	1
SC33	A3880	336.412	-30.619	6.5	168.5	2
SC34	A4059	359.165	-34.999	-65.1	172.1	1
SC35	IIZW108	318.193	2.816	-	-	0

Bibliography

Bellhouse C. et al., 2017, ApJ, 844, 49

Bellhouse C. et al., 2021, MNRAS, 500, 1285

Bellhouse C. et al., 2022, ApJ, 937, 18

Biviano A. et al., 2017, A&A, 607, A81

Boselli A., Gavazzi G., 2006, PASP, 118, 517

Cayatte V., van Gorkom J. H., Balkowski C., Kotanyi C., 1990, AJ, 100, 604

Chung A., van Gorkom J. H., Kenney J. D. P., Crowl H., Vollmer B., 2009, AJ, 138, 1741

Chung A., van Gorkom J. H., Kenney J. D. P., Vollmer B., 2007, ApJ, 659, L115

Cortese L., Catinella B., Smith R., 2021, , 38, e035

Cowie L. L., Songaila A., 1977, Nature, 266, 501

Davies L. J. M. et al., 2019, MNRAS, 483, 5444

Davies R. D., Lewis B. M., 1973, MNRAS, 165, 231

Dey A. et al., 2019, AJ, 157, 168

Dressler A., 1980, ApJ, 236, 351

Dressler A., 1986, ApJ, 301, 35

Ebeling H., Edge A. C., Allen S. W., Crawford C. S., Fabian A. C., Huchra J. P., 2000, MNRAS, 318, 333

Ebeling H., Edge A. C., Böhringer H., Allen S. W., Crawford C. S., Fabian A. C., Voges W., Huchra J. P., 1998, Monthly Notices of the Royal Astronomical Society, 301, 881

Ebeling H., Voges W., Böhringer H., Edge A. C., Huchra J. P., Briel U. G., 1996, Monthly Notices of the Royal Astronomical Society, 281, 799

Fasano G. et al., 2010, MNRAS, 404, 1490

Fasano G. et al., 2006, A&A, 445, 805

Gavazzi G., Contursi A., Carrasco L., Boselli A., Kennicutt R., Scodeggio M., Jaffe W., 1995, A&A, 304, 325

Gavazzi G., Fumagalli M., Cucciati O., Boselli A., 2010, A&A, 517, A73

Giovanelli R., Haynes M. P., 1985, ApJ, 292, 404

Giraud E., 1986, A&A, 167, 25

Gonzalez A. H., Zaritsky D., Zabludoff A. I., 2007, ApJ, 666, 147

Gullieuszik M. et al., 2015, A&A, 581, A41

Gunn J. E., Gott I., J. Richard, 1972, ApJ, 176, 1

Guth A. H., 1981, Phys. Rev. D, 23, 347

Haines C. P. et al., 2015, ApJ, 806, 101

Hubble E., 1926, Contributions from the Mount Wilson Observatory / Carnegie Institution of Washington, 324, 1

Hubble E. P., 1936, Realm of the Nebulae

Jaffé Y. L. et al., 2018, MNRAS, 476, 4753

Jaffé Y. L. et al., 2016, MNRAS, 461, 1202

Kenney J. D. P., Geha M., Jáchym P., Crowl H. H., Dague W., Chung A., van Gorkom J., Vollmer B., 2014, ApJ, 780, 119

Kennicutt J., R. C., 1983, AJ, 88, 483

Kolcu T., Crossett J. P., Bellhouse C., McGee S., 2022, MNRAS, 515, 5877

Kronberger T., Kapferer W., Ferrari C., Unterguggenberger S., Schindler S., 2008, A&A, 481, 337

Larson R. B., Tinsley B. M., Caldwell C. N., 1980, ApJ, 237, 692

Lee J. H., Lee M. G., Mun J. Y., Cho B. S., Kang J., 2022, ApJ, 931, L22

Lin Y.-T., Mohr J. J., 2004, ApJ, 617, 879

Makino J., Hut P., 1997, ApJ, 481, 83

Mather J. C. et al., 1990, ApJ, 354, L37

McPartland C., Ebeling H., Roediger E., Blumenthal K., 2016, MNRAS, 455, 2994

Nulsen P. E. J., 1982, MNRAS, 198, 1007

Ostriker J. P., 1980, Comments on Astrophysics, 8, 177

Peebles P. J. E., 1984, ApJ, 284, 439

Peebles P. J. E., Yu J. T., 1970, ApJ, 162, 815

Planck Collaboration et al., 2020, A&A, 641, A6

Poggianti B. M. et al., 2016, AJ, 151, 78

Poggianti B. M. et al., 2017a, Nature, 548, 304

Poggianti B. M. et al., 2017b, ApJ, 844, 48

Rawle T. D. et al., 2014, MNRAS, 442, 196

Reeves A. M. M., Hudson M. J., Oman K. A., 2022, arXiv e-prints, arXiv:2211.09145

Rhee J., Smith R., Choi H., Yi S. K., Jaffé Y., Candlish G., Sánchez-Jánssen R., 2017, ApJ, 843, 128

Roberts I. D., Parker L. C., 2020a, MNRAS, 495, 554

Roberts I. D., Parker L. C., 2020b, MNRAS, 495, 554

Roberts I. D. et al., 2021a, A&A, 650, A111

Roberts I. D., van Weeren R. J., McGee S. L., Botteon A., Ignesti A., Rottgering H. J. A., 2021b, A&A, 652, A153

Roediger E., Brüggen M., 2006, MNRAS, 369, 567

Roediger E., Brüggen M., 2007, MNRAS, 380, 1399

Roediger E., Bruggen M., Owers M. S., Ebeling H., Sun M., 2014, MNRAS, 443, L114

Roman-Oliveira F., Chies-Santos A. L., Ferrari F., Lucatelli G., Rodríguez Del Pino B., 2021, MNRAS, 500, 40

Sasaki M., 1986, Progress of Theoretical Physics, 76, 1036

Schulz S., Struck C., 2001, MNRAS, 328, 185

Smith R., Fellhauer M., Assmann P., 2012, MNRAS, 420, 1990

Smith R. et al., 2022, ApJ, 934, 86

Smith R. J. et al., 2010, MNRAS, 408, 1417

Solanes J. M., Manrique A., García-Gómez C., González-Casado G., Giovanelli R., Haynes M. P., 2001, ApJ, 548, 97

Tonnesen S., 2019, The Astrophysical Journal, 874, 161

Toomre A., Toomre J., 1972, ApJ, 178, 623

van den Bosch F. C., Aquino D., Yang X., Mo H. J., Pasquali A., McIntosh D. H., Weinmann S. M., Kang X., 2008, MNRAS, 387, 79

Varela J. et al., 2009, A&A, 497, 667

Vulcani B. et al., 2018, MNRAS, 480, 3152

Vulcani B., Poggianti B. M., Smith R., Moretti A., Jaffé Y. L., Gullieuszik M., Fritz J., Bellhouse C., 2022, The Astrophysical Journal, 927, 91

Walker I. R., Mihos J. C., Hernquist L., 1996, ApJ, 460, 121

Warmels R. H., 1988, A&AS, 72, 427

White S. D. M., Rees M. J., 1978, MNRAS, 183, 341

Whitmore B. C., Gilmore D. M., Jones C., 1993, ApJ, 407, 489